

Tritium-Lean Fusion Power Plants with Asymmetric Deuterium-Tritium Transport and Pumping

J. F. Parisi^{1,*}, S. Meschini^{2,3}, A. Rutkowski⁴, and A. Diallo¹

¹*Princeton Plasma Physics Laboratory, Princeton University, Princeton, NJ, USA*

²*Plasma Science and Fusion Center, Massachusetts Institute of Technology, Cambridge, MA, USA*

³*Polytechnic University of Turin, Turin, Piedmont, Italy and*

⁴*Department of Astrophysical Sciences, Princeton University, Princeton, NJ, USA*

Asymmetries in deuterium-tritium (D-T) particle transport and divertor pumping speeds are shown to enhance tritium self-sufficiency in fusion power plants. Using a diffusive particle transport model that links the plasma core, separatrix, and divertor regions, it is shown that reducing tritium transport while increasing deuterium transport improves both tritium burn efficiency and overall fusion power. By selectively increasing deuterium transport, tritium burn efficiency can be further optimized, assuming the availability of asymmetric D-T fueling and advanced divertor technologies. These asymmetries become especially beneficial at high tritium burn efficiencies. In one example, by increasing the D-T particle diffusivity ratio and decreasing the D-T divertor pump speed ratio, each by a factor of five, the tritium burn efficiency increases eleven-fold from 0.026 to 0.29 at fixed fusion power. We propose a novel approach to achieve asymmetric D-T pumping with a divertor re-injection system utilizing a partial ionization plasma centrifuge. In an ARC-class power plant, this approach could yield an order-of-magnitude improvement in tritium burn efficiency. These findings motivate the development of techniques and technologies to reduce core tritium transport and increase tritium divertor pumping speeds.

I. INTRODUCTION

While burning plasma magnetic confinement experiments like ITER and SPARC [1, 2] have not been designed with tritium fuel economy as a priority. For example, ITER is predicted to achieve a burn fraction of only 0.36% [3]. Tritium self-sufficient deuterium-tritium (D-T) fusion power plants will require—and benefit from—substantially higher tritium burn efficiency (TBE) [3–5]. Achieving high TBE in a power plant requires consideration of the core burning plasma, the plasma edge and divertor, and the fueling systems. Optimizing tritium economy presents both physics and engineering challenges, where advances in one area can compensate for lack of progress in another.

Higher TBE offers several advantages. A key benefit is the reduction of on-site tritium inventory, which eases fuel cycle engineering requirements, thereby lowering capital costs and shortening development timelines. Simplified site licensing and regulatory processes are also expected with a smaller tritium inventory, and the reduced tritium inventory lowers the potential for accidental releases into the environment, improving public safety and minimizing ecological contamination risks. Additionally, lower startup inventories would mitigate the risk of global tritium shortages [6–8]. Higher TBE can reduce the required tritium breeding ratios for tritium self-sufficiency [3, 5], while lower tritium particle densities may decrease tritium retention in plasma-facing components and allow a wider range of materials to be considered for plasma-facing components.

In this work, we argue that is desirable for large asymmetries between deuterium and tritium to exist for particle fueling, transport, and pumping. We show how deliberately increasing deuterium particle transport and decreasing tritium particle transport improves the tritium economy of a fusion power plant, provided that sufficient deuterium fueling and pumping is possible in relatively high deuterium particle transport configurations. Therefore, usefully exploiting advances in particle confinement (physics) relies on advances in divertor pumping technology (engineering).

We also argue that departing from a 50:50 D-T fuel ratio – typical for burning D-T fusion system designs [5, 9] – can be advantageous, if not necessary to obtain reasonably high TBE values. It has been suggested that operating a tritium-lean plasma can increase the TBE [10], albeit with a loss in fusion power. Recently, it was suggested that tritium-lean plasmas with spin-polarized fuel could access high TBE without loss of fusion power [11]. In this work, we take another approach, showing simultaneously high TBE and fusion power could be achieved by creating and exploiting asymmetries in D-T particle transport and divertor pumping speeds.

Studies of D-T plasmas in experiments [12–17] and modeling [18–21] have shown that the deuterium and tritium heat and particle transport can be asymmetric, although the results for particle transport are far from definitive. For turbulent ion *heat* transport, the gyroBohm heat diffusivity scaling – $\chi_s \sim \sqrt{m_s}$ for a species s with mass m_s – has additional dependencies that scale as $1/\sqrt{m_s}$ once kinetic electron effects are included [19]. For turbulent ion *particle* transport, it was demonstrated that not only could the deuterium and tritium particle diffusivities differ, $D_D \neq D_T$, but under certain conditions they even have opposite signs, $D_D D_T < 0$ [20].

* jparisi@pppl.gov

Fast ions, electromagnetic effects, $E \times B$ flow shear, and alpha channelling could also play an important role in D-T particle transport asymmetries [19, 21–23]; only in a very limited physical regime – collisionless, electrostatic, single ion, adiabatic electron – does the gyroBohm scaling hold [19]. Given that burning plasmas will have significant fast and impurity ion populations and may have larger electromagnetic fluctuation amplitudes, it is not unreasonable to assume that significant differences in D-T particle transport could arise. Previous work optimized the D-T fuel composition for minimal outflow and exhaust of tritium [24], finding a 2:1 D-T fuel mix was optimal. Recent work has suggested using deuterium flows to sweep out impurities from the plasma core and to provide high tritium confinement [25], thereby enhancing TBE.

In this work, however, we are not concerned with mechanisms that give rise to D-T asymmetries, but the consequences (and opportunities) should such asymmetries exist, leveraging results from [18, 20]. In order to benefit from improved tritium burn efficiency, it is necessary to have a divertor pumping system that preferentially removes tritium. This allows the deuterium divertor particle density to become much larger than the tritium density, improving the TBE.

Asymmetries in pumping naturally arise from the working principles of the pumps. The difference in molecular masses between D_2 and T_2 leads to distinct mean thermal velocities in a D-T gas at temperature T due to the $1/\sqrt{m_s}$ dependence. Since divertor pumping occurs in the kinetic regime, this creates a pumping speed asymmetry. Further asymmetries are introduced by the technological choices in pumping systems. For example, the differing sublimation pressures of D_2 and T_2 impact cryocondensation-based technologies [26]. Additionally, when cryosorption is used, the use of sorbent materials introduces another asymmetry due to differences in sticking probability [27]. Isotopic effects have also been observed in other pumping techniques, such as proton conductor pumps [28] and vapor diffusion pumps [29], although in these cases deuterium is generally faster to pump than tritium due to its lower mass. Given the benefits of asymmetric D-T pumping, there is strong incentive to explore additional techniques for its enhancement.

In Figure 1, we summarize the main effects of variable D-T particle transport and D-T divertor pumping for an ARC-class device with a fusion power of $P_f = 481$ MW. Increasing the D-T particle transport ratio Θ_{DT} and decreasing the D-T divertor volumetric pumping speed ratio Σ_{DT} broadly have similar benefits for increasing the fusion power – this is shown by the progressively increasing Θ_{DT} values and decreasing Σ_{DT} values in Figure 1. Θ_{DT} and Σ_{DT} are defined in Sections II and III respectively. Going from the nominal case ($\Theta_{DT} = 1, \Sigma_{DT} = 1$) to the efficient case ($\Theta_{DT} = 5, \Sigma_{DT} = 1/5$) in Figure 1, the tritium fueling rate decreases by a factor of 11 from $\dot{N}_T^{\text{in}} = 66 \times 10^{20} \text{s}^{-1}$ to $6 \times 10^{20} \text{s}^{-1}$ while maintaining fusion power. Overall, the TBE increases from 0.03 to

0.29.

The main takeaway from Figure 1 is that very high TBE plasmas could be enabled by physics and technology advances in improving and controlling Θ_{DT} and Σ_{DT} . This is discussed in detail in Section VI B.

The layout of this paper is as follows: In Section II, we introduce the model and notation that includes the effects of asymmetric D-T transport. In Section III, we extend the model to also include the effects of asymmetric divertor pumping. In Section IV we consider constraints from vacuum technology and in Section V we consider the results in the context of current technology. We apply the model to an ARC-class power plant in Section VI, focusing on two distinct operating regimes with either high TBE values or high fusion power. We describe potential avenues for developing vacuum and fueling technologies that could facilitate the D-T asymmetric scenarios in Section VII. We summarize in Section VIII.

II. DIFFERENTIAL PARTICLE TRANSPORT

In this section, we introduce the notation for different deuterium and tritium particle fluxes. We assume a three species plasma with deuterium, tritium, and electrons. In this work, we draw extensively from the model originally introduced in [4] and extended to variable tritium fraction in [11]. Our analysis is applicable to the steady-state operation of magnetic confinement devices such as tokamaks, stellarators, and mirrors. The main quantities used in this work are listed in Table III, in the appendix.

A. Core Fuel Mix

We first consider the effect of different deuterium and tritium particle transport on the core D-T fuel mix. The tritium particle flow rate through a flux surface is

$$\dot{N}_T^{\text{co}} = A\Gamma_T, \quad (1)$$

where A is the surface area of a flux surface and Γ_T is the particle flux. We use a diffusive model for the particle flux where fluxes are driven by the density gradient,

$$\Gamma_T = -D_T \nabla n_T^{\text{co}}. \quad (2)$$

Here, D_T is a diffusion coefficient and n_T^{co} is the tritium density. The tritium flow rate \dot{N}_T^{co} is therefore

$$\dot{N}_T^{\text{co}} = -AD_T \nabla n_T^{\text{co}}. \quad (3)$$

It should be noted that non-diffusive processes are often important for particle transport [30, 31], which we have neglected in this analysis but consider in a forthcoming work. The total hydrogen particle flux is

$$\begin{aligned} \dot{N}_Q^{\text{co}} &= \dot{N}_T^{\text{co}} + \dot{N}_D^{\text{co}} \\ &= -A(D_T \nabla n_T^{\text{co}} + D_D \nabla n_D^{\text{co}}). \end{aligned} \quad (4)$$

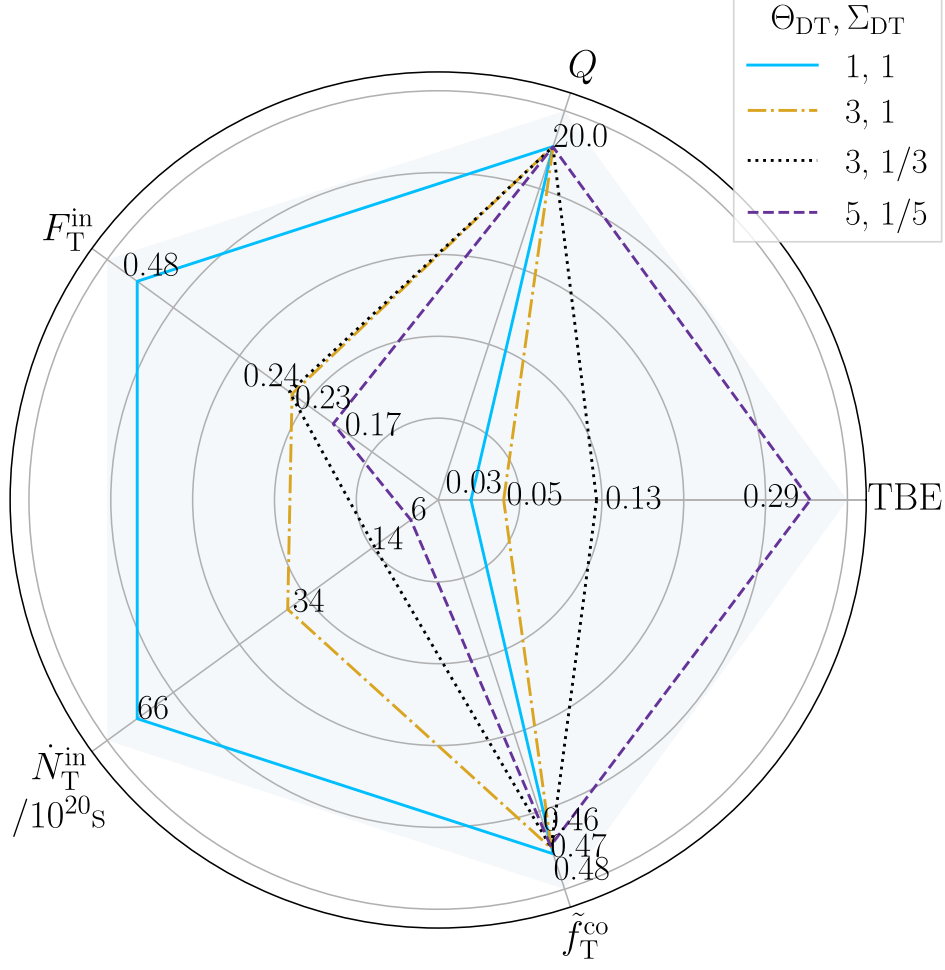
ARC-class Power Plant, Constant $P_f = 481$ MW

FIG. 1: Tritium self-sufficiency and fusion power parameters of an ARC-class device for four cases with high fusion power $P_f = 481$ MW: The D-T transport ratio is Θ_{DT} (Equation (7)), the D-T pumping speed ratio is Σ_{DT} (Equation (47)) the tritium flow rate injection fraction is F_T^{in} (Equation (11)), the tritium fueling rate is \dot{N}_T^{in} , the plasma gain is Q , and the typical tritium core density fraction is \tilde{f}_T^{co} (Equation (35)). All axes have a value of zero at the origin and are linearly scaled.

Here, \dot{N}_D^{co} , D_D , n_D^{co} are the core flow rate, diffusivity, and density for deuterium. Substituting $n_D^{co} = n_T^{co} (1 - f_T^{co}) / f_T^{co}$, in Equation (4), where the tritium core density fraction is

$$f_T^{co} \equiv n_T^{co} / n_Q^{co}, \quad (5)$$

where $n_Q^{co} = n_D^{co} + n_T^{co}$ is the hydrogen fuel density, gives

$$\dot{N}_Q^{co} = -AD_T \nabla n_T^{co} \left(1 + \Theta_{DT} \frac{\Lambda - f_T^{co}}{f_T^{co}} \right). \quad (6)$$

Here, the core D-T particle diffusivity ratio is

$$\Theta_{DT} \equiv D_D / D_T, \quad (7)$$

and the core tritium-to-hydrogen logarithmic density gradient ratio is

$$\Lambda \equiv L_{n,T} / L_{n,Q}, \quad (8)$$

where the logarithmic density gradient is $L_{n,T} \equiv -(\partial_r \ln n_T)^{-1}$, which is a typical quantity used in gyrokinetic stability and transport analysis [32–35]. Another useful quantity is the tritium core flow rate fraction

$$F_T^{co} \equiv \dot{N}_T^{co} / \dot{N}_Q^{co}. \quad (9)$$

Using Equations (3) and (6), Equation (9) becomes

$$F_T^{co} = \frac{f_T^{co}}{\Theta_{DT} (\Lambda - f_T^{co}) + f_T^{co}}. \quad (10)$$

In the limit of equal deuterium and tritium diffusivity and $\Lambda = 1$, Equation (10) reduces to $F_T^{co} = f_T^{co}$, which was the limit used in [11].

We do not explicitly impose the constraint from ambipolarity of the turbulent particle fluxes: $\sum_s Z_s \Gamma_s = 0$ for a sum over species $s \in [e, D, T]$. Because ambipolarity must always be satisfied, we assume that Γ_e may vary as we consider variations in Γ_D and Γ_T .

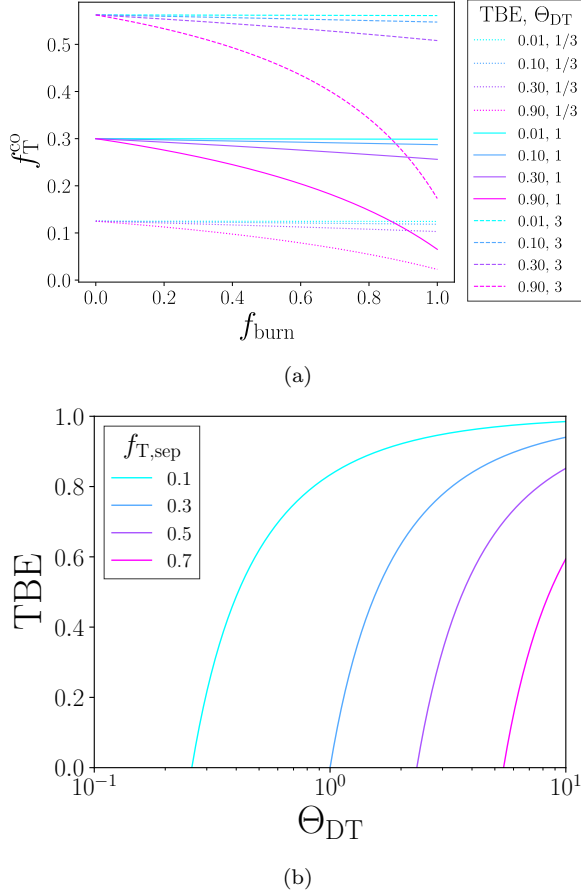


FIG. 2: (a) Tritium core fraction f_T^{co} (Equation (18)) versus enclosed burn fraction f_{burn} for different tritium burn efficiency (TBE, Equation (20)) TBE versus Θ_{DT} values. (b) TBE versus Θ_{DT} . Here, $\Lambda = 1$ and $F_T^{\text{in}} = 0.3$.

B. Tritium Burn Efficiency

In this subsection, we relate core transport to tritium burn efficiency.

The tritium fraction F_T^{in} of the fueling rate is

$$F_T^{\text{in}} \equiv \dot{N}_T^{\text{in}} / \dot{N}_Q^{\text{in}}, \quad (11)$$

where \dot{N}_T^{in} and \dot{N}_Q^{in} are the particle fueling rates for tritium and total hydrogen fuel. The tritium fraction F_T^{div} of the unburned hydrogen fuel removal rate in the divertor is

$$F_T^{\text{div}} \equiv \dot{N}_T^{\text{div}} / \dot{N}_Q^{\text{div}}, \quad (12)$$

where \dot{N}_T^{div} and \dot{N}_Q^{div} are the number of tritium and total unburned fuel particle removal flow rates. The tritium enrichment H_T measures the relative tritium flow rate in the divertor compared with the core,

$$H_T \equiv F_T^{\text{div}} / F_T^{\text{in}}. \quad (13)$$

We now define \dot{N}_T^{co} (Equation (1)) as the tritium flow rate through a flux surface that encloses a fraction f_{burn}

of the total fusion power,

$$\dot{N}_T^{\text{co}} \equiv \dot{N}_T^{\text{in}} - f_{\text{burn}} \dot{N}_T^{\text{burn}}, \quad (14)$$

where \dot{N}_T^{co} also satisfies

$$\dot{N}_Q^{\text{co}} \equiv \dot{N}_Q^{\text{in}} - 2f_{\text{burn}} \dot{N}_T^{\text{burn}}. \quad (15)$$

Equations (14) and (15) are derived in Appendix B of [11]. Here, \dot{N}_T^{burn} is the tritium burn rate across the entire plasma. By introducing the radial coordinate f_{burn} , we have introduced a radial dependence to the problem with f_{burn} : on the magnetic axis $f_{\text{burn}} = 0$ and on the separatrix $f_{\text{burn}} = 1.0$. Equations (14) and (15) describe a model where all of the deuterium and tritium fuel is injected on the magnetic axis. We ignore other particle sources such as particles re-entering the plasma core from the scrape-off layer. Dividing Equation (14) by Equation (15) gives

$$F_T^{\text{co}} = F_T^{\text{in}} \frac{1 - f_{\text{burn}} \text{TBE}}{1 - 2f_{\text{burn}} F_T^{\text{in}} \text{TBE}}. \quad (16)$$

Because F_T^{in} and TBE are scalars and f_{burn} is a flux function, F_T^{co} is also a flux function. The tritium burn efficiency (TBE) [4] is defined as

$$\text{TBE} \equiv \frac{\dot{N}_T^{\text{burn}}}{\dot{N}_T^{\text{in}}} = \left(\frac{\dot{N}_T^{\text{div}}}{\dot{N}_{\text{He}}^{\text{div}}} + 1 \right)^{-1}, \quad (17)$$

which physically represents the probability of a tritium atom undergoing fusion between its injection into the plasma and its removal through the divertor exhaust. Here, $\dot{N}_{\text{He}}^{\text{div}}$ is the helium ash removal rate. Equating Equations (10) and (16), f_T^{co} is

$$f_T^{\text{co}} = \frac{\Lambda \Theta_{\text{DT}} (f_{\text{burn}} \text{TBE} - 1)}{f_{\text{burn}} \text{TBE} (1 + \Theta_{\text{DT}}) + 1 - \Theta_{\text{DT}} - 1/F_T^{\text{in}}}. \quad (18)$$

We plot solutions to Equation (18) in Figure 2(a), showing how f_T^{co} decreases with increasing f_{burn} , increasing TBE, and decreasing Θ_{DT} (at fixed F_T^{in}).

Defining the tritium density fraction at the separatrix,

$$f_T^{\text{sep}} \equiv f_T^{\text{co}}(f_{\text{burn}} = 1), \quad (19)$$

and rearranging Equation (18) with $f_{\text{burn}} = 1$ for the TBE, we find

$$\text{TBE} = 1 + \frac{f_T^{\text{sep}} (1 - 2F_T^{\text{in}})}{f_T^{\text{sep}} F_T^{\text{in}} (1 + \Theta_{\text{DT}}) - F_T^{\text{in}} \Lambda \Theta_{\text{DT}}}. \quad (20)$$

Solutions to the TBE in Equation (20) are shown in Figure 2(b): decreasing f_T^{sep} and increasing Θ_{DT} are beneficial to the TBE.

In our model, the tritium particle diffusivity scales as

$$|D_T| \sim \frac{1}{A} \frac{\dot{N}_T^{\text{co}}}{\nabla n_T^{\text{co}}} = \frac{1}{A} \frac{\dot{N}_T^{\text{in}} - f_{\text{burn}} \dot{N}_T^{\text{burn}}}{\nabla n_T^{\text{co}}}. \quad (21)$$

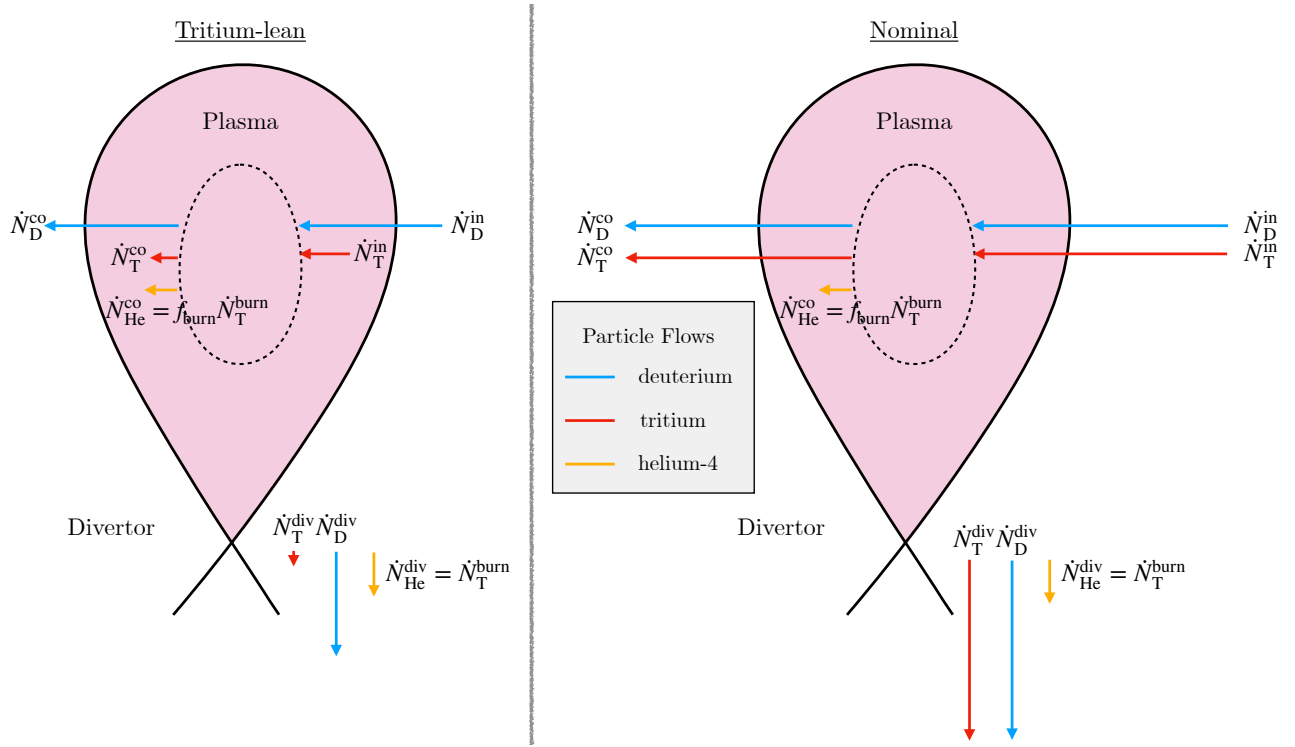


FIG. 3: Schematic of the particle flows in a tritium-lean and a nominal configuration, both at equal total fusion power. The dashed flux surface in the plasma is described by the flux coordinate f_{burn} (Equation (14)). The arrows' magnitudes represent the size of the particle flows. In the tritium-lean case, the tritium flows are significantly smaller than the deuterium flows.

Using the definition of the TBE,

$$|D_T| \sim \frac{1}{A} \frac{\dot{N}_T^{\text{burn}} \left(\frac{1}{\text{TBE}} - f_{\text{burn}} \right)}{\nabla n_T^{\text{co}}}, \quad (22)$$

the relative diffusivities scale as

$$\Theta_{DT} \sim \left(1 + \frac{1}{F_T^{\text{in}}} \frac{1 - 2F_T^{\text{in}}}{1 - f_{\text{burn}} \text{TBE}} \right) \frac{L_{n_D}}{L_{n_T}} \frac{f_T^{\text{co}}}{1 - f_T^{\text{co}}}. \quad (23)$$

Given that we are generally interested in $F_T^{\text{in}} < 1/2$ (in order to obtain high TBE), higher TBE with all other variables constant in Equation (23) requires higher Θ_{DT} . This is shown in Figure 2(b) where for fixed f_T^{sep} , $\Lambda = 1$, and $F_T^{\text{in}} = 0.3$, the value of Θ_{DT} increases with TBE. We will show in Section VI E that for fixed fusion power, increases in Θ_{DT} that maximize the TBE come from D_T decreasing and D_D increasing by equal factors.

Using the TBE definition in Equation (17), we relate the TBE to H_T , F_T^{div} , and F_T^{in} ,

$$H_T = \frac{1 - \text{TBE}}{1 - 2F_T^{\text{in}} \text{TBE}}, \quad (24)$$

where conservation of particles requires

$$\dot{N}_Q^{\text{in}} = 2\dot{N}_T^{\text{burn}} + \dot{N}_Q^{\text{div}} \quad (25)$$

and

$$\dot{N}_T^{\text{in}} = \dot{N}_T^{\text{burn}} + \dot{N}_T^{\text{div}}. \quad (26)$$

A schematic for this system of equations is shown in Figure 3. The right figure corresponds to a nominal case where the deuterium and tritium flows are equal. The left figure corresponds to a tritium-lean case where the tritium flows are significantly reduced. Notably, we will see that the total deuterium flows also decrease in tritium-lean configurations.

III. DIFFERENTIAL PUMPING

In this section, we couple core transport and divertor pumping to find expressions for the TBE and fusion power.

A. Tritium Burn Efficiency

The divertor flow rate for a species x is given by the neutral gas density n_x^{div} and effective pumping speed S_x [4],

$$\dot{N}_x^{\text{div}} = n_x^{\text{div}} S_x. \quad (27)$$

It will be helpful to define the helium-to-tritium pumping speed,

$$\Sigma_{\text{HeT}} = S_{\text{He}}/S_T, \quad (28)$$

and the divertor density ratio

$$f_{\text{HeT,div}} = n_{\text{He}}^{\text{div}}/n_{\text{T}}^{\text{div}}. \quad (29)$$

Using Equations (17), (28) and (29), we obtain a simple expression for the TBE,

$$\text{TBE} = \frac{f_{\text{HeT,div}}\Sigma_{\text{HeT}}}{1 + f_{\text{HeT,div}}\Sigma_{\text{HeT}}}. \quad (30)$$

Equation (30) shows that if Σ_{HeT} is held constant, the only way to change the TBE is to change the helium to tritium density fraction. As explained in [4], the TBE increases monotonically with $f_{\text{HeT,div}}\Sigma_{\text{HeT}}$. In this paper, we hold Σ_{HeT} constant, and therefore any increase in TBE comes from increasing $f_{\text{HeT,div}}$. This paper describes new ways to increase $f_{\text{HeT,div}}$. Techniques for increasing Σ_{HeT} are left for future works, although the techniques for changing Σ_{DT} will likely also apply to Σ_{HeT} .

Why does increasing $f_{\text{HeT,div}}\Sigma_{\text{HeT}}$ also increase the tritium burn efficiency? If the fusion power is constant,

$$\begin{aligned} f_{\text{HeT,div}}\Sigma_{\text{HeT}} &\sim \frac{1}{\dot{N}_{\text{T}}^{\text{div}}} = \frac{1}{\dot{N}_{\text{T}}^{\text{in}} - \dot{N}_{\text{T}}^{\text{burn}}} \sim \frac{1}{\dot{N}_{\text{T}}^{\text{co}}} \\ &\sim \frac{1}{D_{\text{T}}} \sim \text{TBE}. \end{aligned} \quad (31)$$

Therefore, increasing $f_{\text{HeT,div}}\Sigma_{\text{HeT}}$ corresponds to a decrease in tritium particle flux $\dot{N}_{\text{T}}^{\text{co}}$ due to a lower D_{T} value. Thus, increasing $f_{\text{HeT,div}}\Sigma_{\text{HeT}}$ does not causally increase the TBE, but rather, is a necessary divertor condition for reduced tritium particle transport in the plasma core.

B. Fusion Power

We now calculate the effect of differential D-T pumping speeds on the fusion power. The helium-to-electron core density ratio [4] is,

$$f_{\text{dil}} \equiv n_{\alpha}^{\text{co}}/n_e^{\text{co}}, \quad (32)$$

where n_{α}^{co} and n_e^{co} are the core alpha and electron densities. Using quasineutrality without impurities,

$$n_e^{\text{co}} = n_Q^{\text{co}} + 2n_{\alpha}^{\text{co}}, \quad (33)$$

the power density at the flux surface $f_{\text{burn}} = 1/2$ is

$$\tilde{p}_f = 4\tilde{f}_{\text{T}}^{\text{co}}(1 - \tilde{f}_{\text{T}}^{\text{co}})(1 - 2f_{\text{dil}})^2 (n_e^{\text{co}})^2 \langle v\bar{\sigma} \rangle \frac{E}{4}, \quad (34)$$

where n_e^{co} is the electron density, $\langle v\bar{\sigma} \rangle$ is the fusion reactivity, and we have defined

$$\tilde{f}_{\text{T}}^{\text{co}} \equiv f_{\text{T}}^{\text{co}}(f_{\text{burn}} \equiv 1/2), \quad (35)$$

so $\tilde{f}_{\text{T}}^{\text{co}}$ describes the flux surface that encloses half of the power fusion power, $f_{\text{burn}} = 1/2$. Thus, at fixed n_e^{co}

and temperature, the fusion power density \tilde{p}_f relative to its maximum value $p_{f,max}$ where $p_{f,max}$ has $\tilde{f}_{\text{T}}^{\text{co}} = 1/2$, $f_{\text{dil}} = 0$, is given by the power multiplier p_{Δ}

$$p_{\Delta} \equiv \frac{\tilde{p}_f}{p_{f,max}} = 4\tilde{f}_{\text{T}}^{\text{co}}(1 - \tilde{f}_{\text{T}}^{\text{co}})(1 - 2f_{\text{dil}})^2. \quad (36)$$

We now find an expression for f_{dil} . An important quantity is the helium enrichment, the ratio of the helium-to-fuel density ratios in the divertor and core,

$$\eta_{\text{He}} \equiv f_{\text{He,div}}/f_{\alpha,\text{co}}, \quad (37)$$

where the helium-to-fuel divertor density ratio is

$$f_{\text{He,div}} \equiv \frac{n_{\text{He}}^{\text{div}}}{n_{\text{Q}}^{\text{div}}} = \frac{f_{\text{HeT,div}}}{1 + f_{\text{DT,div}}}, \quad (38)$$

the helium-to-fuel density ratio in the core is

$$f_{\alpha}^{\text{co}} \equiv n_{\alpha}^{\text{co}}/n_{\text{Q}}^{\text{co}}, \quad (39)$$

and the deuterium-to-tritium divertor density ratio is

$$f_{\text{DT,div}} = n_{\text{D}}^{\text{div}}/n_{\text{T}}^{\text{div}}. \quad (40)$$

Combining Equations (36) to (39) we obtain

$$p_{\Delta} = 4\tilde{f}_{\text{T}}^{\text{co}}(1 - \tilde{f}_{\text{T}}^{\text{co}}) \left[1 - \left(1 + \frac{\eta_{\text{He}}}{2f_{\text{He,div}}} \right)^{-1} \right]^2, \quad (41)$$

where we used

$$f_{\text{dil}} = \frac{f_{\text{He,div}}/\eta_{\text{He}}}{1 + 2f_{\text{He,div}}/\eta_{\text{He}}}. \quad (42)$$

We use

$$f_{\text{HeT,div}} = \frac{1}{\Sigma_{\text{HeT}}} \frac{1}{\frac{1}{\text{TBE}} - 1}, \quad (43)$$

$f_{\text{He,div}}$ (Equation (38)), and p_{Δ} (Equation (41)) to find

$$p_{\Delta} = \frac{4\tilde{f}_{\text{T}}^{\text{co}}(1 - \tilde{f}_{\text{T}}^{\text{co}})}{\left[1 - \frac{2}{\eta_{\text{He}}\Sigma_{\text{HeT}}(1 + f_{\text{DT,div}})\left(1 - \frac{1}{\text{TBE}}\right)} \right]^2}. \quad (44)$$

Applying the boundary condition for equal flow rates at the separatrix and divertor,

$$F_{\text{T}}^{\text{sep}} = F_{\text{T}}^{\text{div}} = \frac{1}{1 + f_{\text{DT,div}}\Sigma_{\text{DT}}}, \quad (45)$$

gives (using Equation (10))

$$\frac{f_{\text{T}}^{\text{sep}}}{\Theta_{\text{DT}}(\Lambda - f_{\text{T}}^{\text{sep}}) + f_{\text{T}}^{\text{sep}}} = \frac{1}{1 + f_{\text{DT,div}}\Sigma_{\text{DT}}}, \quad (46)$$

where the deuterium-to-tritium pumping speed ratio is

$$\Sigma_{\text{DT}} \equiv S_{\text{D}}/S_{\text{T}}. \quad (47)$$

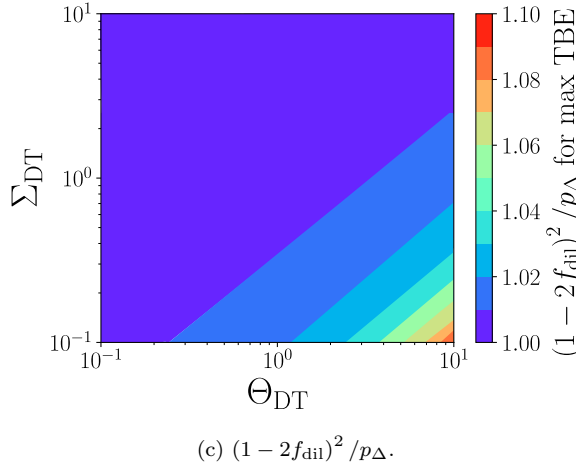
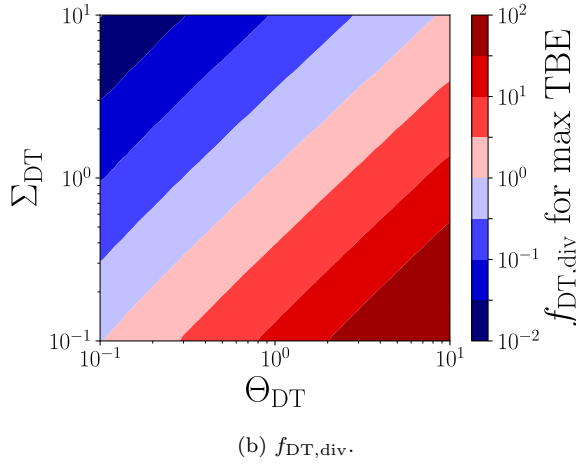
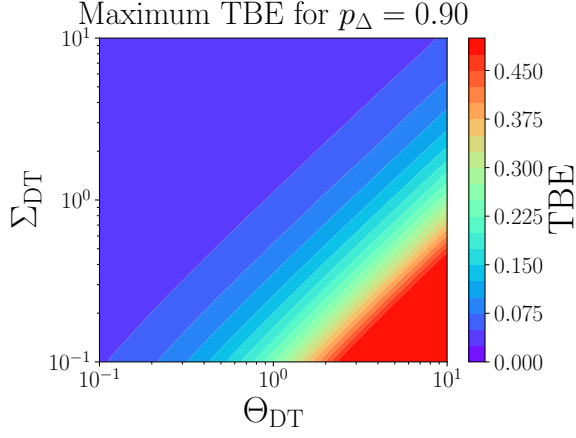


FIG. 4: Results of numerical scheme to maximize TBE for fixed fusion power multiplier $p_\Delta = 0.90$. (a): Maximum achievable TBE versus Θ_{DT} and Σ_{DT} . (b): corresponding $f_{DT,div}$. (c): corresponding $(1 - 2f_{dil})^2 / p_\Delta$.

Rearranging Equation (46) gives

$$f_{DT,div} = \frac{\Theta_{DT}}{\Sigma_{DT}} \frac{\Lambda - f_T^{sep}}{f_T^{sep}}. \quad (48)$$

$f_{DT,div}$ is an important quantity: by increasing $f_{DT,div}$

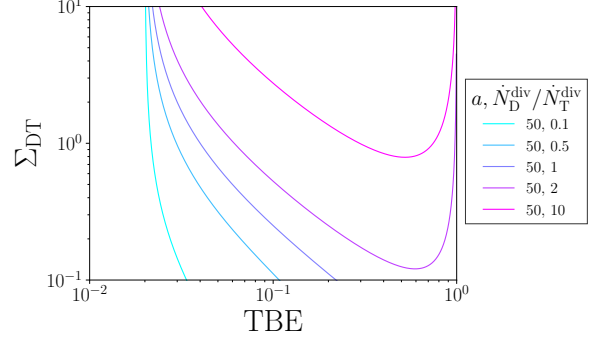
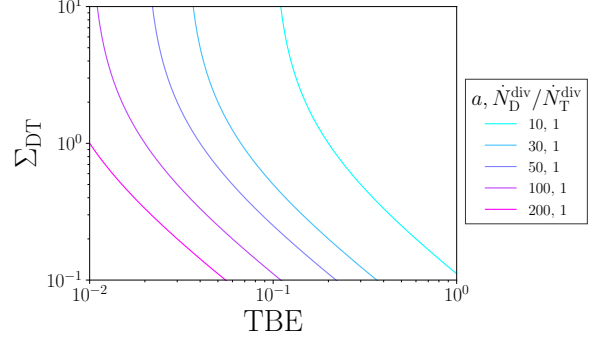


FIG. 5: Required Σ_{DT} versus TBE using approximations in Equations (51) and (52) for fixed fusion power and assuming $TBE \ll 1$.

through smaller Σ_{DT} and larger Θ_{DT} values, the fusion power can be maintained while the TBE is increased. When p_Δ is fixed, per Equation (34), this means that $\tilde{f}_T^{co}(1 - \tilde{f}_T^{co})(1 - 2f_{dil})^2$ is also fixed. At relatively low TBE values and fixed power, the terms $\tilde{f}_T^{co}(1 - \tilde{f}_T^{co})$ and $(1 - 2f_{dil})^2$ individually vary little with Σ_{DT} and larger Θ_{DT} . This is shown in Figure 4 (c). Therefore, assuming f_{dil} is fixed, from Equation (38)

$$TBE / \Sigma_{HeT} \sim f_{HeT,div} = f_{He,div} (1 + f_{DT,div}), \quad (49)$$

where $f_{He,div}$ is constant and independent of $f_{DT,div}$. Given that $f_{DT,div}$ increases strongly with smaller Σ_{DT} and larger Θ_{DT} (see Figure 4 (b)), Equation (49) implies that $f_{HeT,div}$ also increases. According to Equation (30), the TBE only depends on $f_{HeT,div}$ and Σ_{HeT} , the latter we hold fixed. Therefore, by increasing $f_{DT,div}$, $f_{HeT,div}$ also increases, increasing the TBE. This argument holds until relatively large TBE values, when holding p_Δ constant requires both $\tilde{f}_T^{co}(1 - \tilde{f}_T^{co})$ and $(1 - 2f_{dil})^2$ to individually vary.

It is important to distinguish the effect of Θ_{DT} from Σ_{DT} . Using Equation (31) that $f_{HeT,div} \Sigma_{HeT} \sim 1 / \dot{N}_T^{co}$ and Equation (49),

$$1 + \frac{1}{\Sigma_{DT}} \Theta_{DT} \frac{\Lambda - f_T^{sep}}{f_T^{sep}} \sim \frac{1}{\dot{N}_T^{co}} \sim \frac{1}{D_T \nabla n_T^{co}}. \quad (50)$$

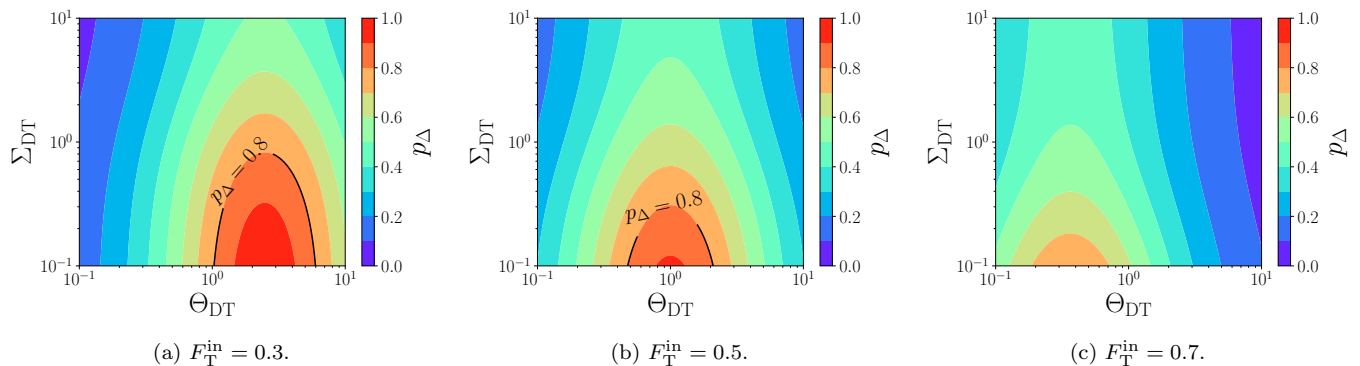


FIG. 6: Fusion power multiplier p_Δ versus Θ_{DT} and Σ_{DT} for three F_T^{in} values. In all figures, $\Lambda = \Sigma_{\text{HeT}} = \eta_{\text{He}} = 1.0$, $\text{TBE} = 0.2$.

Therefore, at fixed power, $\Theta_{DT} (\Lambda - f_T^{\text{sep}}) / f_T^{\text{sep}}$, and n_T^{co} , any decreases in D_T must have a corresponding decrease in Σ_{DT} as the TBE increases. Physically, as the D-T particle diffusivities decrease, the power plant operator may choose to decrease the D-T fueling, which decreases the divertor particle flow rate. Because this increases the TBE at fixed power due to lower required fueling (for both D and T), the D-T divertor density $f_{DT,\text{div}}$ will increase. However, the ratio of tritium-to-deuterium flow rates at the divertor has not changed significantly i.e. $f_{DT,\text{div}} \Sigma_{DT}$ is approximately constant. Thus, Σ_{DT} must decrease. The required Σ_{DT} value can also be written as

$$\Sigma_{DT} = \frac{1}{f_{DT,\text{div}}} \frac{\dot{N}_D^{\text{in}} / \dot{N}_T^{\text{in}} - \text{TBE}}{1 - \text{TBE}}. \quad (51)$$

Using the arguments surrounding Equation (49) to write $f_{DT,\text{div}}$ at fixed fusion power as

$$f_{DT,\text{div}} = a \text{TBE} - 1, \quad (52)$$

we can approximately capture the behavior of Σ_{DT} in Equation (51). In Equation (52), $a = 1/f_{\text{He},\text{div}} \Sigma_{\text{HeT}} \gg 1$. Figure 5 shows solutions to Equations (51) and (52) versus TBE. For large regions of parameter space, access to high TBE regimes without decreasing fusion power requires low values of Σ_{DT} .

To summarize: decreasing Σ_{DT} and increasing Θ_{DT} increases the TBE while maintaining fusion power. This increases the relative amount of deuterium to tritium in the divertor, $f_{DT,\text{div}}$, which also increases the amount of helium relative to tritium in the divertor $f_{\text{HeT},\text{div}}$. As assumed throughout this paper, the helium-to-tritium pumping speed Σ_{HeT} is fixed. Therefore, the increase in $f_{\text{HeT},\text{div}}$ increases the TBE (Equation (30)). Using Σ_{DT} and Θ_{DT} allows us to simultaneously increase $f_{\text{HeT},\text{div}}$ and $f_{DT,\text{div}}$, keeping $f_{\text{He},\text{div}}$ and f_{dil} roughly constant. If we could not vary Σ_{DT} and Θ_{DT} , increases in $f_{\text{HeT},\text{div}}$ (and therefore TBE) are much larger than increases in $f_{DT,\text{div}}$, meaning that the plasma becomes more diluted through f_{dil} (Equation (42)) and therefore the power decreases. With technology that allows smaller Σ_{DT} values,

the fusion power can be sustained as the TBE increases through smaller $f_{DT,\text{div}}$.

We summarize numerical results to support the above arguments. Shown in Figure 4(a), we plot the maximum TBE versus Θ_{DT} and Σ_{DT} for fixed $p_\Delta = 0.90$ (Equation (44)). The maximization in the TBE is performed by searching over all possible F_T^{in} and selecting the F_T^{in} that gives the highest TBE value, subject to all other quantities in the system being physical. As expected, smaller Σ_{DT} and larger Θ_{DT} values increase the TBE. This is achieved by order of magnitude increases in $f_{DT,\text{div}}$, shown in Figure 4(b). In Figure 4(c), we plot the power dilution term $(1 - 2f_{\text{dil}})^2 / p_\Delta$ – apart from exceptionally large Θ_{DT} and very small Σ_{DT} , the quantity $(1 - 2f_{\text{dil}})^2 / p_\Delta$ is very close to 1, indicating that f_{dil} changes slowly across Θ_{DT} , Σ_{DT} space – and therefore the assumption of fixed $f_{\text{He},\text{div}}$ at fixed power (used in Equation (49)) is often valid. Only when the TBE no longer satisfies $\text{TBE} \ll 1$ is $(1 - 2f_{\text{dil}})^2 / p_\Delta$ slightly larger than 1.

Solutions to p_Δ in Equation (44) are shown in Figure 6: each subplot corresponds to a different F_T^{in} value. For all subplots, TBE, Λ , and Σ_{HeT} are fixed. For these parameters, decreasing Σ_{DT} always allows a high power, and the optimal Θ_{DT} value depends on F_T^{in} . However, smaller F_T^{in} values are more desirable if larger Θ_{DT} values are achievable. Given that the TBE in these plots is fixed, for a given p_Δ , the tritium injection flow rate \dot{N}_T^{in} is also the same for all plots. Therefore, when varying F_T^{in} at fixed TBE and fixed p_Δ , \dot{N}_D^{in} is changing but \dot{N}_T^{in} is fixed. This explains why at lower F_T^{in} (higher \dot{N}_D^{in}), a larger Θ_{DT} is necessary to more quickly remove deuterium from the core with the benefit of higher fusion power.

We now consider key quantities for an optimization scheme where the maximum power is found for a fixed TBE value. The optimization is performed over F_T^{in} . In the top row of Figure 7, we plot p_Δ as a function of Θ_{DT} and Σ_{DT} for fixed η_{He} , Σ_{HeT} , for three TBE values. Increasing Θ_{DT} and decreasing Σ_{DT} gives higher p_Δ ; the effect on p_Δ is particularly strong at higher TBE values, indicating the importance of Θ_{DT} and Σ_{DT} in

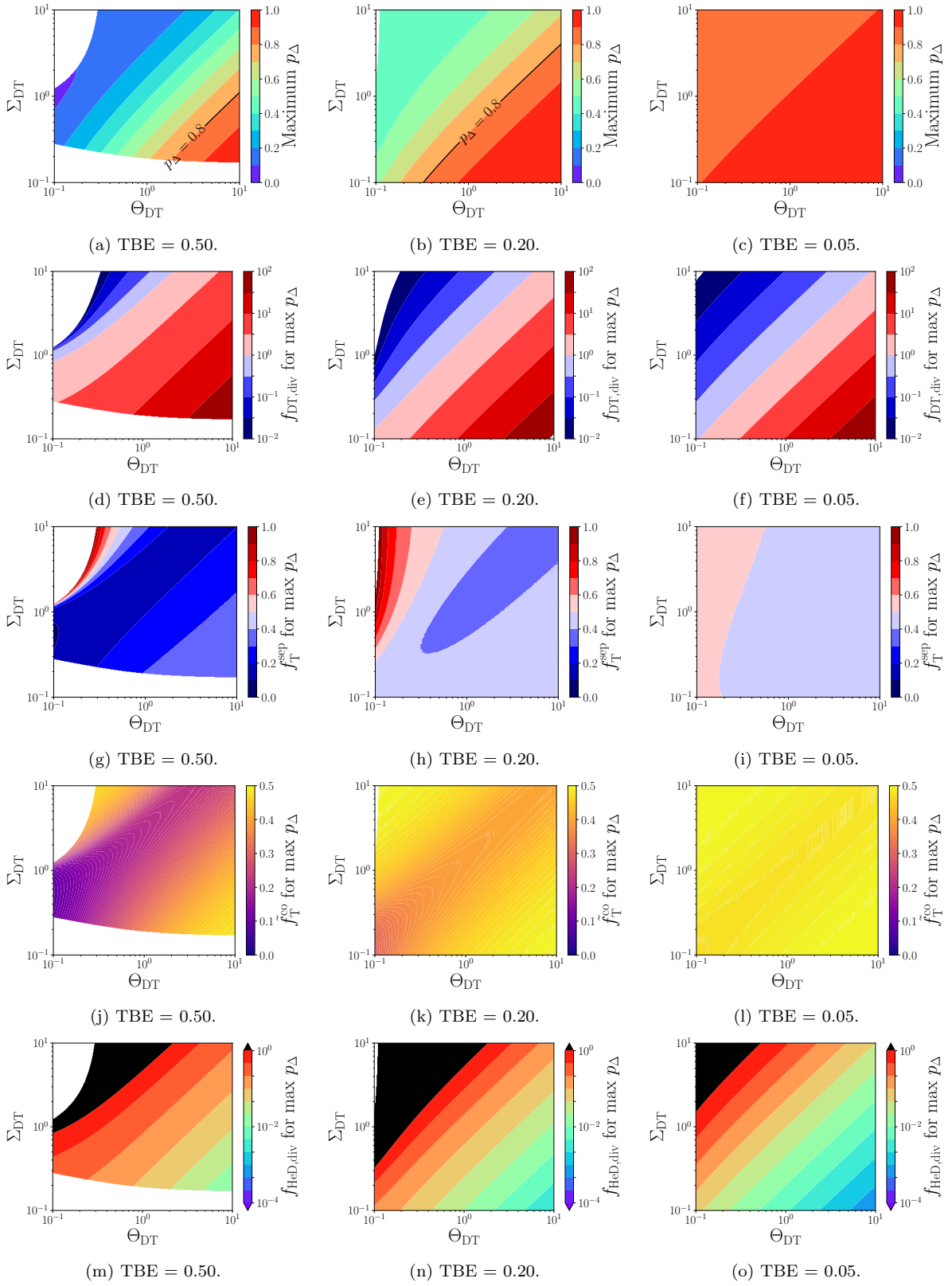


FIG. 7: Figures of merit versus Θ_{DT} and Σ_{DT} . First row: fusion power multiplier p_{Δ} , second row: $f_{DT,div}$, third row f_T^{sep} , fourth row f_T^{co} , fifth row $f_{HeD,div}$: In all plots, $\Sigma_{HeT}\eta_{He} = 0.5$, and F_T^{in} is the value that maximizes p_{Δ} .

tritium-efficient regimes. In the remaining four rows, we show $f_{DT,div}$, f_T^{sep} , f_T^{co} , and $f_{He,div}$. Writing the TBE in

Equation (30) to leading order as

$$\text{TBE} \approx f_{\text{HeT},\text{div}} \Sigma_{\text{HeT}} = f_{\text{HeD},\text{div}} f_{\text{DT},\text{div}} \Sigma_{\text{HeD}} \Sigma_{\text{DT}}, \quad (53)$$

and using $f_{\text{DT},\text{div}}$ in Equation (48) we find

$$\text{TBE} \approx f_{\text{HeD},\text{div}} \frac{\Sigma_{\text{HeT}} \Theta_{\text{DT}} (\Lambda - f_{\text{T}}^{\text{sep}})}{\Sigma_{\text{DT}} f_{\text{T}}^{\text{sep}}}. \quad (54)$$

From Equation (54), given that $\text{TBE} \geq 0$, we must enforce $\Lambda \geq f_{\text{T}}^{\text{sep}}$. Assuming that Σ_{HeD} , Θ_{DT} , and Λ are fixed, TBE increases by increasing $f_{\text{HeD},\text{div}}$ and decreasing $f_{\text{T}}^{\text{sep}}$. Comparing the three columns in the third row of Figure 7, at higher TBE the $f_{\text{T}}^{\text{sep}}$ values are smaller. Additionally, at fixed TBE we generally see that increasing Θ_{DT} corresponds to decreasing $f_{\text{T}}^{\text{sep}}$ (unless TBE is very large), in agreement with Equation (54); this only fails to hold when Θ_{DT} is small and Σ_{DT} is large (and therefore $\Sigma_{\text{HeD}} = \Sigma_{\text{HeT}}/\Sigma_{\text{DT}}$ is small at fixed Σ_{HeT}). Comparing $f_{\text{HeD},\text{div}}$ in the final row of Figure 7 shows how higher values of $f_{\text{HeD},\text{div}}$ at higher TBE, as expected from Equation (54).

It is important to keep in mind the consequences of fixed Σ_{HeT} when varying Σ_{DT} . Because

$$\Sigma_{\text{HeT}} = \Sigma_{\text{HeD}} \Sigma_{\text{DT}}, \quad (55)$$

the product $\Sigma_{\text{HeD}} \Sigma_{\text{DT}}$ must be fixed. We find advantageous regimes for $\Sigma_{\text{DT}} < 1$, requiring faster volumetric pumping for the heavier isotope, T. However, as Σ_{DT} is decreased there must be a corresponding increase in $\text{Sigma}_{\text{HeD}}$, which again, requires the heavier element, He, to be pumped faster than deuterium.

C. Fusion Gain

In this section, we study the effects of differential deuterium-tritium transport and pumping on the fusion plasma gain Q .

Power balance in the core approximately requires

$$p_{\alpha} (1 + 5/Q) = \frac{w_{\text{th}}}{\tau_E}, \quad (56)$$

where p_{α} is the alpha heating power density, $Q = p_f/p_{\text{heat}}$ is the plasma fusion gain on a flux surface, p_{heat} is the heating power density absorbed by the plasma, τ_E is the energy confinement time and w_{th} is the stored thermal energy density. Expressing the core thermal energy density as

$$w_{\text{th}} = \frac{3}{2} (n_e^{\text{co}} + n_Q^{\text{co}}) k_B T + \frac{3}{2} n_{\alpha}^{\text{co}} k_B \langle T_{\alpha} \rangle, \quad (57)$$

where the alpha particle pressure is

$$w_{\text{th},\alpha} = \frac{3}{2} n_{\alpha} k_B \langle T_{\alpha} \rangle, \quad (58)$$

and the temperature $\langle T_{\alpha} \rangle$ is an average over alpha particle energies. Here, electron and ion temperatures have an

equal value T . Using quasineutrality, $n_Q^{\text{co}} = n_e^{\text{co}} - 2n_{\alpha}^{\text{co}}$, Equation (58) is

$$w_{\text{th}} = 3k_B T M, \quad (59)$$

where the dilution factor is

$$M \equiv \left(1 + f_{\text{dil}} \left(\frac{1}{2} \frac{\langle T_{\alpha} \rangle}{T} - 1 \right) \right), \quad (60)$$

which is equal to 1 when there are no helium dilution effects. We obtain

$$n_e \tau_E (1 + 5/Q) = \frac{15k_B T}{\langle v \bar{\sigma} \rangle E/4} C, \quad (61)$$

where

$$C \equiv \frac{1 + f_{\text{dil}} \left(\frac{1}{2} \frac{\langle T_{\alpha} \rangle}{T} - 1 \right)}{4 \tilde{f}_{\text{T}}^{\text{co}} (1 - \tilde{f}_{\text{T}}^{\text{co}}) (1 - 2f_{\text{dil}})^2}, \quad (62)$$

is the required multiplier to keep Q constant at fixed T . For simplicity, in this work we use $\langle T_{\alpha} \rangle = T$ as in [4], although the effect of different $\langle T_{\alpha} \rangle$ values is presented in Appendix D3 in [11].

We now show the effects of Θ_{DT} and Σ_{DT} on C . In Figure 8, we plot the C values corresponding to the three TBE values in Figure 7 (TBE=0.50,0.20,0.05) versus Θ_{DT} and Σ_{DT} for three TBE values. At higher TBE values, TBE = 0.50 in Figure 8(a), there are two regions for a C minimum with the Θ_{DT} and Σ_{DT} values we consider (however, the upper spatial region in Figure 8(a) is undesirable because the fusion power is very low), but at lower TBE values, there is a single C minimum region in Θ_{DT} and Σ_{DT} . The results in Figure 8 showing higher Θ_{DT} and lower Σ_{DT} increasing the fusion gain further reinforce the trend we find of higher Θ_{DT} and lower Σ_{DT} to be desirable for fusion power.

IV. VACUUM PUMPING

In this section, we briefly review vacuum pumping and relate pumping speed to the main divertor quantities introduced above.

The throughput Q_{pump} of a vacuum pump is

$$Q_{\text{pump}} \equiv pS = \dot{N} k_B T \quad (63)$$

where p is the pressure at the pump inlet, S is the volumetric pumping speed, \dot{N} is the atomic or molecular flow rate, k_B is the Boltzmann constant and T is the temperature. Note that the pump throughput is typically reported in units of $\text{Pa m}^3 \text{s}^{-1}$ instead of W, and is usually referenced to the standard temperature $T_{\text{st}} = 273.15 \text{ K}$.

The ideal pumping speed of a pump is

$$S_{\text{id}} = A_p \frac{\bar{c}}{4}, \quad (64)$$

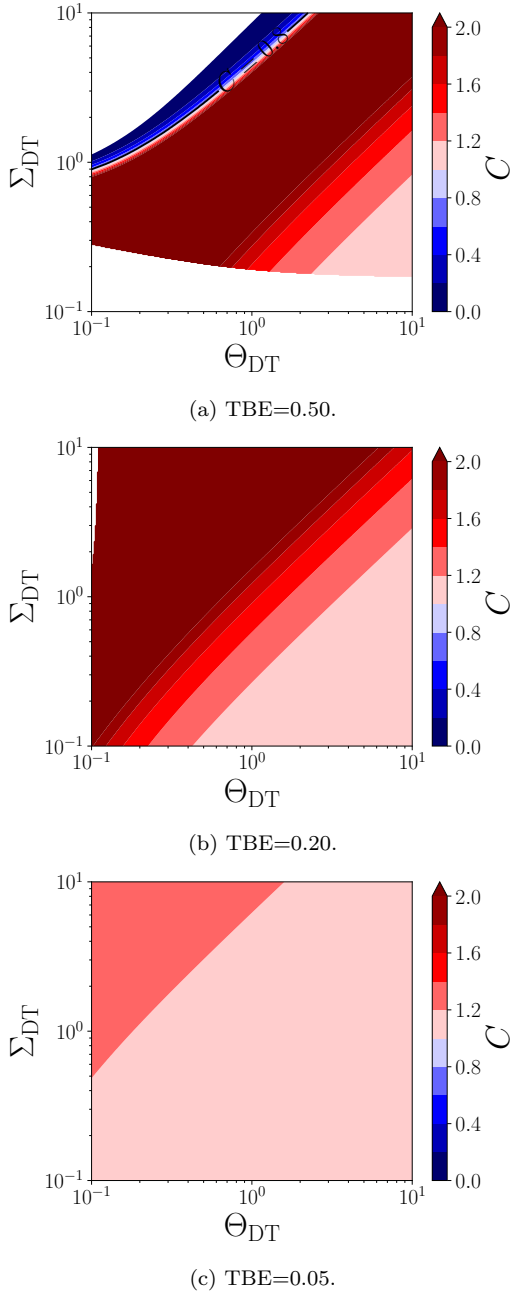


FIG. 8: Required $n_e\tau E$ multiplication factor C (Equation (62)) versus Θ_{DT} , Σ_{HeT} to maintain a fixed plasma gain. Lower C values indicate a higher fusion gain.

where \bar{c} is the mean gas velocity and A_p is the cross sectional area of the pump. Assuming a Maxwell-Boltzmann distribution, $\bar{c} = \sqrt{8RT/\pi M}$ where M is the molar mass of the gas and R is the ideal gas constant. This (kinetic) approach is valid in the free molecular flow regime.

In a real vacuum system, the gas experiences different flow regimes (free molecular, transitional, and viscous), and can be described by the Knudsen number $\text{Kn} \equiv \lambda/d$ where d is the effective molecular diameter and λ is the gas particle mean free path. A high Knudsen ($\text{Kn} \gtrsim 10$)

indicates a free molecular flow. This is the case for the primary vacuum pumps (i.e., torus pumps). Therefore, ideal relations can be derived between pumping speeds for different species (e.g., species x and y). Assuming an equal temperature for x and y , Equation (64) gives

$$\frac{S_x}{S_y} = \sqrt{\frac{M_y}{M_x}}. \quad (65)$$

Considering that hydrogenic species are found as molecules (Q_2 in the divertor neutrals region), while helium is in atomic form, from Equation (65):

$$\frac{S_{D_2}}{S_{He}} = 1, \quad (66)$$

and

$$\frac{S_{T_2}}{S_{He}} = \frac{S_{T_2}}{S_{D_2}} = \sqrt{\frac{2}{3}}. \quad (67)$$

Neglecting for simplicity the differences in capture coefficient, the relation between the pumping speeds of different species is given by Eqs. (66) and (67). The total pumping speed provided by N_p pumps is:

$$S_{\text{tot}} = \frac{N_p Q_{\text{pump}}}{p_{\text{div}}} = N_p (n_T^{\text{div}} S_{T,\text{div}} + n_D^{\text{div}} S_{D,\text{div}} + n_{He}^{\text{div}} S_{He,\text{div}}) \frac{k_B T}{p_{\text{div}}}, \quad (68)$$

that can be rewritten as:

$$S_{\text{tot}} = N_p \dot{N}_T^{\text{div}} \frac{k_B T}{p_{\text{div}}} \times \left(1 + f_{DT,\text{div}} \Sigma_{DT} + f_{He,\text{div}} \Sigma_{HeT} \right), \quad (69)$$

again assuming that all species have an equal temperature.

Using these results, we can find \dot{N}_T^{div} as a function of just two variables: $f_{DT,\text{div}}$ and $f_{He,\text{div}}$. Considering that: S_{tot} is limited by the pump performance; Equations (66) and (67) prescribe the relative pumping speeds; $k_B T/p_{\text{div}}$ can be considered a constant ($T = T_{\text{st}}$ and $p_{\text{div}} \sim 1 - 10 \text{ Pa}$); and the number of pumps N_p is constrained by geometrical considerations; Equation (69) provides a relation between $(\dot{N}_T^{\text{div}}, f_{DT,\text{div}}, f_{He,\text{div}})$ and engineering parameters. Figure 9 shows the maximum allowable tritium flux through the divertor by using 6 pumps with $S_{\text{tot}} = 50 \text{ m}^3 \text{ s}^{-1}$ (typical pumping speed of vapor diffusion pumps) as a function of $f_{DT,\text{div}}$, $f_{He,\text{div}}$.

Equation (69) can be related to core transport by using

$$\dot{N}_T^{\text{div}} \simeq \dot{N}_T^{\text{sep}} = -AD_T \nabla n_T^{\text{co}} \Big|_{\text{sep}}, \quad (70)$$

allowing one to link the radial profile of n_T^{co} with the pumping speed and the divertor densities of D, T, and He.

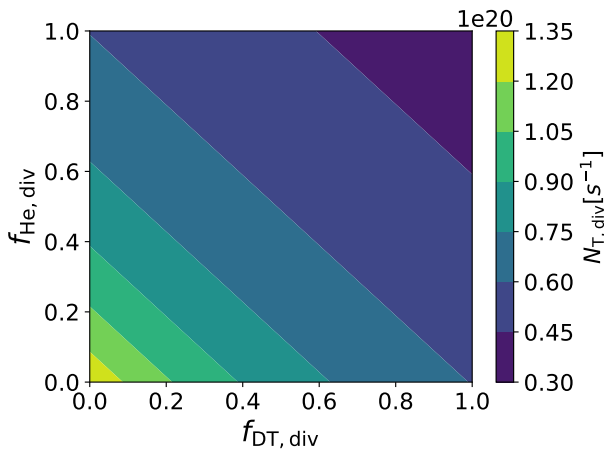


FIG. 9: Maximum exhausted tritium flow rate versus $f_{\text{DT,div}}$ and $f_{\text{He,div}}$. Here, $S_{\text{tot}} = 50 \text{ m}^3 \text{ s}^{-1}$ and $p_{\text{div}} = 5 \text{ Pa}$.

V. COMPARISON WITH EXISTING TECHNOLOGY

In this section, we briefly review the new results in this paper in the context of current fuel cycle technologies. Most fuel cycle designs have focused on operations with a 50:50 D-T ratio, as this ratio maximizes fusion power density and, at low TBE, results in an exhaust stream with a similar ratio, facilitating direction internal recycling (DIR) operations [36]. However, in this work, we demonstrated that operating at a low F_{T}^{in} and leveraging asymmetric deuterium-tritium transport and pumping lead to (a) a significant enhancement in TBE, and (b) a much broader operating space for D-T fractions, both in the core and in the divertor. It is important to evaluate how these novel operational schemes affect fuel cycle design and how existing technologies constrain the parameter space presented in Section II.

A. Fueling system

Fueling schemes anticipated for ITER and modern fusion devices primarily rely on fuel pellet injection. Fuel pellets can be produced by pipe guns, which also provide pellet acceleration, or by extruders, with the latter being preferred for their ability to produce a larger number of pellets over extended periods. The pellets produced by the extruder are then accelerated using gas guns (single or two-stage), mechanical centrifuges, electro-thermal accelerators, or electro-magnetic rail guns [37]. No significant issues are expected when operating at different D-T injection ratios. Extruders are capable of producing pellets with any D-T mixture. Similarly, the performance of pellet injectors is not affected by the D-T mixture. While operating with a rapidly changing D-T fraction may be challenging due to the timescales associated with the ex-

trusion process (on the order of minutes), maintaining operation around a steady-state value, even at very low tritium fractions, appears feasible with current technologies [38].

An important constraint in the fueling system comes from the maximum amount of tritium contained in a given volume [39], e.g., the extruder. Therefore, operations at low F_{T}^{in} are beneficial for tritium management and safety. Table I shows the relevant fuel cycle parameters for an ARC-class FPP. A design implementing differential transport and pumping ($\Theta_{\text{DT}} = 5$, $\Sigma_{\text{DT}} = 1/5$, $F_{\text{T}}^{\text{in}} = 0.17$) achieves a TBE of 29%, and a total particle flow rate $\dot{N}_{\text{tot,in}} = \dot{N}_{\text{T}}^{\text{in}} + \dot{N}_{\text{D}}^{\text{in}} = 3.5 \times 10^{21} \text{ s}^{-1}$, or $Q_{\text{tot,in}} = 13.1 \text{ Pa m}^3 \text{ s}^{-1}$. For a similar FPP operating without differential transport and pumping ($\Theta_{\text{DT}} = 1$, $\Sigma_{\text{DT}} = 1$, $F_{\text{T}}^{\text{in}} = 0.48$), TBE = 3%, the total particle flow rate is much higher $\dot{N}_{\text{tot,in}} = 1.4 \times 10^{22} \text{ s}^{-1}$, or $Q_{\text{tot,in}} = 51.6 \text{ Pa m}^3 \text{ s}^{-1}$. Thanks to the TBE improvements achieved by D-T asymmetric transport and pumping, both the total flow rate and the tritium flow rate are lower, despite the fractional increase in D flow rate. Thus, tritium-lean plasmas also tend to be deuterium-lean.

B. Exhaust pumping

In Section IV we computed $\dot{N}_{\text{T}}^{\text{div}}$ for an ideal vacuum pump. It should be noted that in a real pump additional factors can affect the pumping speed. The non-ideal behaviour of a real pump is accounted for by the capture coefficient, c_{capt} :

$$c_{\text{capt}} = \frac{S_{\text{real}}}{S_{\text{id}}}, \quad (71)$$

where S_{real} is the real pump speed. The capture coefficient is therefore computed from experimental tests or detailed simulations of the pump operations. For a cryopump, in addition to the geometry and the flow regime, c_{capt} depends on the sticking coefficient (c_{stick}) of the different species in the exhaust stream. For a typical charcoal cryosorbent (e.g., the one used in ITER), $c_{\text{stick,He}} = 0.1$, $c_{\text{stick,D}_2} = 0.88$, and $c_{\text{stick,T}_2} = 1$ [40], resulting in higher pumping speed for D and T than He. For a vapor diffusion pump, the capture coefficient depends on the interaction between the gas with the vapor jet, with lighter elements showing a lower capture coefficient due to increased backflow through the jet, with He achieving higher pumping speeds than T2 [29]. These simple considerations highlight how differential pumping is strongly driven by the technology (and the underlying physical principles) employed in the torus pumping, and the limitations of an ideal pumping approach.

Common pumping speeds for candidate primary pumping technology are $50 - 80 \text{ m}^3 \text{ s}^{-1}$ for cryopumps, $50 - 70 \text{ m}^3 \text{ s}^{-1}$ for vapor diffusion pumps, and $1 - 3 \text{ m}^3 \text{ s}^{-1}$ for turbomolecular pumps. However, practical considerations (e.g., tritium safety) limits the throughput of

cryopumps, resulting in a much lower effective pumping speed. For instance, in ITER cryopumps the surface saturation of charcoal is reached at a gas load of 0.5 Pa m^3 per cm^2 of sorbent surface. Each cryopump has 28 baffles coated with charcoal, for a total adsorbing surface of 11.2 m^2 per pump [41]. Considering a throughput of $\sim 200 \text{ Pa m}^3 \text{ s}^{-1}$ [42], and 6 cryopumps, the time before regeneration due to saturation of the sorbent is:

$$\Delta t_{\text{sat}} = 0.5 \frac{N_{\text{p}} A_{\text{sorbent}}}{Q_{\text{pump}}} \sim 1100 \text{ s}, \quad (72)$$

while the time before regeneration due to hydrogen flammability limit (in a volume $V \sim 6 \text{ m}^3$ as per ITER cryopumps [43], and a maximum allowable partial pressure of $p_{\text{H}_2, \text{max}} = 1.7 \text{ kPa}$ [44]) is:

$$\Delta t_{\text{flamm}} = \frac{p_{\text{H}_2, \text{max}} V}{Q_{\text{pump}}} \sim 50 \text{ s}, \quad (73)$$

or, stated in another way, for Δt of interest for FPPs, the throughput of a cryopump is $\sim 20\times$ less than the one predicted by considering the cryosorbent saturation as limiting factor. Note also that Δt_{flamm} depends on the partial pressure of all the hydrogenic species, not just tritium. Increasing $f_{\text{He, div}}$ or Σ_{HeT} is an effective way to reduce the throughput and, consequently, to increase the operating time of the cryopump before regeneration is needed. Instead, decreasing the tritium fraction relative to the other hydrogen species does not provide benefits unless the hydrogen throughput decreases, as the bottleneck for operations is the flammability limit and not the tritium inventory in the cryopump.

For the values in Table I, referring to the same cases of Section V A, for a device using differential transport and pumping the total flow rate through the exhaust system is $\dot{N}_{\text{tot}}^{\text{div}} = \dot{N}_{\text{T}}^{\text{div}} + \dot{N}_{\text{D}}^{\text{div}} + \dot{N}_{\text{He}}^{\text{div}} = 3.3 \times 10^{21} \text{ s}^{-1}$, or $Q_{\text{pump}} = 12.4 \text{ Pa m}^3 \text{ s}^{-1}$. If we compare these values to a standard 50:50 D-T burn scheme, the total flow rate through the exhaust system is $\dot{N}_{\text{tot}}^{\text{div}} = 1.4 \times 10^{22} \text{ s}^{-1}$, or $Q_{\text{pump}} = 51.1 \text{ Pa m}^3 \text{ s}^{-1}$.

Therefore, the throughput is reduced by $\sim 5\times$ with asymmetric D-T transport and pumping, which is also reflected in the lower I_{startup} . From the perspective of pumping requirements, the reduced tritium content enhances radiological safety, while the lower throughput extends the pump's operating time before regeneration is necessary (both Equation (72) and Equation (73) shows a Q_{pump}^{-1} dependence for Δt). Similarly, turbomolecular pumps may be capable of providing the required throughput when operating with asymmetric D-T transport and pumping, provided they can be made tritium compatible.

It should be noted that the required throughput must account for additional factors related to plasma control and operations (e.g., gas injection in the divertor region). Therefore, the throughput reported here does not guarantee that these technologies can be applied under the

conditions described in Table I (machine-specific considerations must be made), but it does illustrate how asymmetric D-T transport and pumping can ease some of the demands on the torus pumping system.

C. Direct Internal Recycling

The efficacy of DIR depends on its ability to directly recycle D and T with minimal processing time, delivering them to the gas distribution system before fueling them back in the fusion system. Similar D-T ratios at injection and exhaust allows for a short processing time, with the option of adjusting the mixture in the gas distribution system [45]. However, if the exhaust D-T ratio differs significantly from that at fueling, an isotope rebalancing system may be needed, increasing the processing time of the DIR, limiting its effectiveness. For fuel pellet injection

$$F_{\text{T}}^{\text{in}} = \frac{\dot{N}_{\text{T}}^{\text{in}}}{\dot{N}_{\text{Q}}^{\text{in}}} = \frac{n_{\text{T}}^{\text{in}}}{n_{\text{Q}}^{\text{in}}} = \frac{1}{1 + f_{\text{DT}}^{\text{in}}}, \quad (74)$$

because the speed of the two species (D and T) is the same, and equals the pellet speed. This means that the D-T fueling ratio is prescribed once F_{T}^{in} is fixed. $f_{\text{DT, div}}$ depends instead on both $F_{\text{T}}^{\text{div}}$ and Σ_{DT} :

$$F_{\text{T}}^{\text{div}} = \frac{1}{1 + f_{\text{DT, div}} \Sigma_{\text{DT}}}. \quad (75)$$

When $\Sigma_{\text{DT}} \simeq 1$, DIR operations are mostly unaffected if $F_{\text{T}}^{\text{in}} \simeq F_{\text{T}}^{\text{div}}$ (i.e., $H_{\text{T}} \simeq 1$). However, when Σ_{DT} differs significantly from 1, the optimal value of H_{T} for DIR operations changes. For the values in Table I ($\Sigma_{\text{DT}} = 1/5$, $f_{\text{T}}^{\text{sep}} = 0.43$, and $H_{\text{T}} = 0.13/0.17 = 0.76$). However, because DIR requires $F_{\text{T}}^{\text{in}} = F_{\text{T}}^{\text{sep}}$, using $F_{\text{T}}^{\text{in}} \simeq F_{\text{T}}^{\text{div}}$, DIR operates with $H_{\text{T}} \simeq 1.0$. Therefore, it is not certain whether the tritium-lean plasmas described here are compatible with DIR.

In terms of operations, the D-T ratio may or may not affect the performance of candidate technologies [46, 47]. For metal foil pumps, plasma-driven permeation through Nb foils has been shown to exhibit no isotopic effect between H_2 and D_2 [45]. Conversely, proton-conducting pumps do show isotope effects, indicating that their efficiency may vary depending on the D-T fuel mix [28].

D. Tritium processing plant

Operating at very high TBE changes some of the paradigms in fuel cycle dynamics. The critical role of the tritium processing plant (referred to as the inner fuel cycle in [42, 48]) in achieving tritium self-sufficiency is evident since at low TBE, the tritium fueling flow rate significantly exceeds the tritium burned, with most of it being exhausted. For instance, at $\text{TBE} = 2\%$, $\dot{N}_{\text{T}}^{\text{in}} = 50 \dot{N}_{\text{T, burn}}$

and $\dot{N}_T^{\text{div}} = 49\dot{N}_{T,\text{burn}}$. This results in high I_{startup} , and, consequently, in high TBR_r . Strategies that shorten the residence (processing) time of tritium in the tritium plant prove to be very effective because they impact $\sim 98\%$ of the total tritium re-circulating in the plant.

Operating at high TBE with asymmetric D-T transport and pumping (assume $\text{TBE} = 60\%$ as in Table I) has two major effects: (a) the amount of tritium injected is comparable to the tritium burnt ($\dot{N}_T^{\text{in}} = 1.2\dot{N}_{T,\text{burn}}$), greatly reducing I_{startup} , and (b) the amount of tritium exhaust is even lower than the tritium burnt ($\dot{N}_T^{\text{div}} = 0.6\dot{N}_{T,\text{burn}}$). Considering that the tritium extracted from the outer fuel cycle (i.e., the breeding blanket, tritium extraction system, and, potentially, heat exchangers) is, roughly speaking, $\text{TBR} \cdot \dot{N}_{T,\text{burn}}$, the impact of the design parameters of outer fuel cycle components (residence times, tritium extraction efficiency, tritium losses, etc.) becomes comparable to those of the inner fuel cycle, which is not the case for low TBE operations (see for instance the parametric analysis in [42, 48]). In general, reducing the tritium flow rate through the reprocessing plant enables a broader set of technologies, including those with longer residence times, should they provide benefits in terms of other performance metrics (e.g., purity level of the streams).

In this section, we have reviewed the current technological capabilities of fueling systems, exhaust pumping, direct internal recycling, and tritium processing. Developing pumps with asymmetric D-T pumping is a high priority, and we present such a scheme in Section VII. Direct internal recycling may not be needed with asymmetric D-T transport and pumping. Generally, operating at higher TBE allows a wider range of tritium processing technologies to be considered.

VI. ARC-CLASS STUDY

In this section, we show the effect of differential deuterium-tritium transport and pumping on an ARC-class power plant. We consider two main regimes: high fusion power and high TBE. We then perform dedicated scans in Σ_{DT} , Θ_{DT} , and Σ_{DT} and Θ_{DT} simultaneously in order to clarify the separate effects of Σ_{DT} and Θ_{DT} .

Our nominal case for the ARC-class fusion system has $\text{TBE} = 0.026$, $P_f = 481$ MW, $Q = 20$, and a startup tritium inventory of 0.40 kg [5]. Note that this is a higher TBE than the nominal case described in [11] because in this work we use a more optimistic value of $\Sigma_{\text{HeT}} = 1.0$ whereas in [11] $\Sigma_{\text{HeT}} = 0.63$. For all of the cases in this section, either the TBE or fusion power is maximized by finding the optimal value of F_T^{in} .

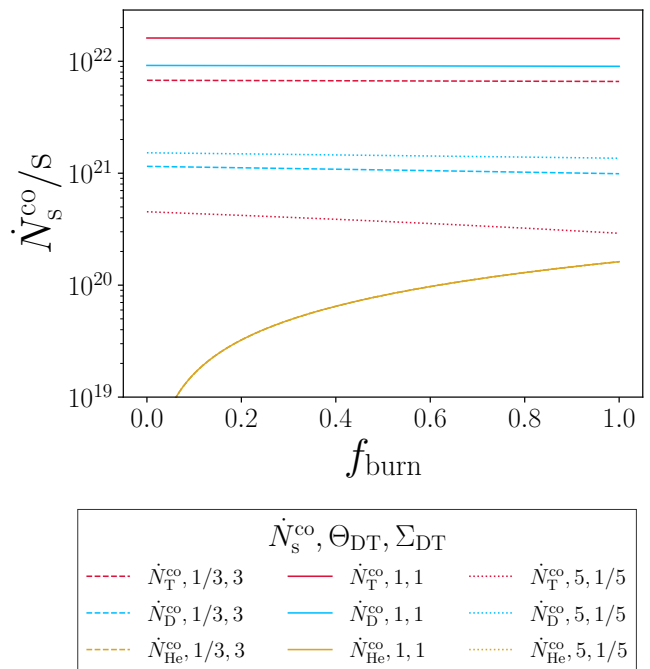


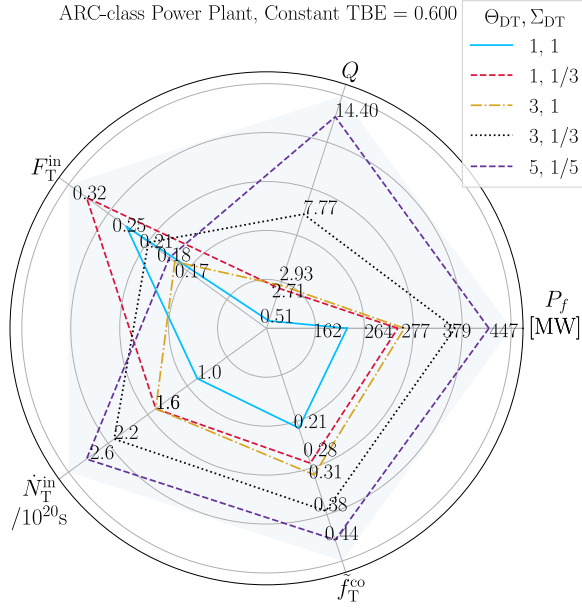
FIG. 10: Radial dependence of deuterium, tritium, and helium flows for three ARC-class cases at fixed fusion power described in Section VI A.

A. High Fusion Power

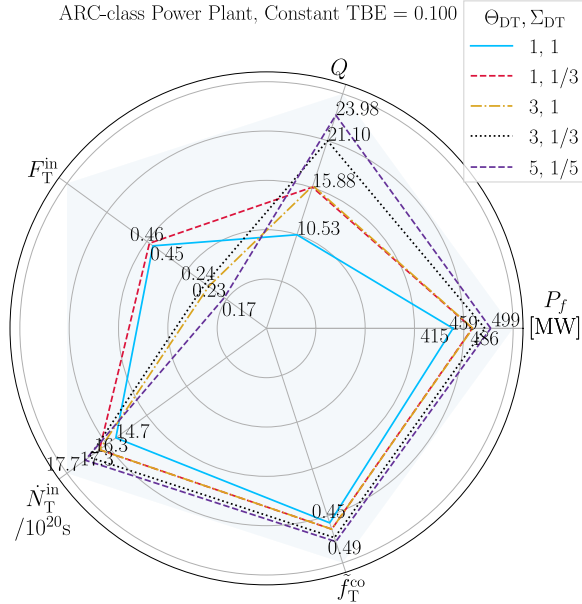
In this subsection, we study a high power ARC-class fusion system with $P_f = 481$ MW. By high power, we mean that the power degradation is relatively small ($p_\Delta = 0.95$), which corresponds to lower TBE values. The tritium input fraction F_T^{in} is chosen to maximize the TBE at fixed power. Figure 1 shows the corresponding spider diagram. There is a 30-fold decrease in the required tritium fueling from the nominal to the leanest tritium case ($\Theta_{\text{DT}} = 5$, $\Sigma_{\text{DT}} = 1/5$), and the TBE increases from 0.01 to 0.36. Previous results have shown that TBE increases with lower \tilde{f}_T^{co} [10, 11]. This work shows that by preferentially transporting deuterium and pumping tritium, one obtains higher \tilde{f}_T^{co} while still running a tritium-lean power plant. Shown in Table I, at very large Θ_{DT} and small Σ_{DT} , the amount of injected and divertor-pumped tritium and deuterium *both* decrease. This indicates that tritium-lean power plants may also be more deuterium-efficient.

To further illustrate the significant differences between these cases with constant fusion power, in Figure 10 we plot the radial dependence of the deuterium, tritium, and helium particle flows. There is an almost two order of magnitude reduction in the tritium flows in the tritium-lean case compared with the nominal and tritium-abundant cases. Because the fusion power is constant, there is no difference in the helium flows.

Further details are listed in Table I. $I_{\text{startup},\text{min}}$ is the minimum tritium startup inventory according to [5].



(a) TBE=0.60.



(b) TBE=0.10.

FIG. 11: Tritium self-sufficiency and fusion power parameters of an ARC-class device for five cases with very high tritium burn efficiency (TBE) = 0.60 (a) and moderate TBE = 0.10 (b): The D-T transport ratio is Θ_{DT} (Equation (7)), the D-T pumping speed ratio is Σ_{DT} (Equation (47)), the fusion power is P_f , the tritium flow rate injection fraction is F_T^{in} (Equation (11)), the plasma gain is Q_{plas} , the tritium fueling rate is \dot{N}_T^{in} , and the typical tritium fraction is f_T^{co} (Equation (35)). All axes except for Q have a value of zero at the origin and are linearly scaled.

In summary, at high fusion power (481 MW, $p_{\Delta} = 0.95$) we find that while the nominal ARC-class plant only achieves TBE = 0.026, with significant decreases

in particle transport and divertor pumping, much higher TBE is attainable; we showed a tritium-lean case achieving TBE = 0.29.

B. High TBE

In this subsection, we study the effect of Θ_{DT} and Σ_{DT} at high TBE values. At such high TBE values, the importance of Θ_{DT} and Σ_{DT} increases significantly.

Figure 11 shows two spider diagrams for an ARC-class case with very high TBE = 0.60 (Figure 11(a)) and moderate TBE = 0.10 (Figure 11(b)).

For very high TBE = 0.60, the fusion power and gain are very sensitive to Θ_{DT} and Σ_{DT} : as Θ_{DT} increases and Σ_{DT} decreases, the plasma gain and fusion power increase. The blue line shows the case with $\Theta_{DT} = \Sigma_{DT} = 1$ and TBE = 0.60. This is not a viable plasma for a power plant: the gain is only $Q = 0.58$ and the power is only 162 MW. Although not shown in the table, with $\Theta_{DT} = 1/3$ and $\Sigma_{DT} = 3$, the plasma produces only 38 MW of fusion power. Therefore, it is important that $\Theta_{DT} \gtrsim 1$ and $\Sigma_{DT} \lesssim 1$, otherwise the TBE and/or fusion power will be very poor.

Increasing $\Theta_{DT} \rightarrow 5$ and decreasing $\Sigma_{DT} \rightarrow 1/5$, the power increases to 447 MW. In this case, the deuterium divertor density is 51 times higher than the tritium divertor density, $f_{D,T,\text{div}} = 51$ and the tritium and deuterium injection rates are relatively modest at $\dot{N}_T^{\text{in}} = 2.7 \times 10^{20}/\text{s}$ and $\dot{N}_D^{\text{in}} = 12.5 \times 10^{20}/\text{s}$. We can estimate the hydrogen divertor density from Equation (27),

$$n_Q^{\text{div}} = \frac{\dot{N}_D^{\text{div}}}{S_D} + \frac{\dot{N}_T^{\text{div}}}{S_T}. \quad (76)$$

We use the value of $S_{\text{tot}} = 50 \text{ m}^3 \text{ s}^{-1}$ from Section IV to motivate using a tritium pumping speed $S_T = 50 \text{ m}^3 \text{ s}^{-1}$. Given that $\Sigma_{DT} = 1/5$, the deuterium pumping speed is $S_{\text{tot}} = 10 \text{ m}^3 \text{ s}^{-1}$. Using the values of $\dot{N}_D^{\text{div}} = 10.9 \times 10^{20}/\text{s}$ and $\dot{N}_T^{\text{div}} = 1.1 \times 10^{20}/\text{s}$ from Table I, we find $n_Q^{\text{div}} = 1.1 \times 10^{20}/\text{m}^3$. This separatrix density is comparable to the MANTA-class device design with $n_{e,\text{sep}} = 0.9 \times 10^{20}/\text{m}^3$ [49] – the main difference being that for the MANTA-class device $f_{D,T,\text{div}} \simeq 1$ whereas in our example $f_{D,T,\text{div}} = 51$.

However, at moderate TBE values, TBE = 0.10, Θ_{DT} and Σ_{DT} have a much weaker effect on the fusion power. The difference in fusion power for the most pessimistic and optimistic cases we consider, $\Theta_{DT} = 1/3$ and $\Sigma_{DT} = 3$ and $\Theta_{DT} = 5$ and $\Sigma_{DT} = 1/5$, is much smaller: the former has $P_f = 351$ and the latter $P_f = 499$ MW.

In summary, we have shown that power plants with extremely high TBE – here, TBE = 0.60, may be attained with very large Θ_{DT} and very small Σ_{DT} . Compared with the nominal transport and pumping parameters $\Theta_{DT} = 1$ and $\Sigma_{DT} = 1$, a power plant with $\Theta_{DT} = 5$ and $\Sigma_{DT} = 1/5$ is predicted to achieve a fusion power that is nearly three times higher (447 MW versus 162 MW).

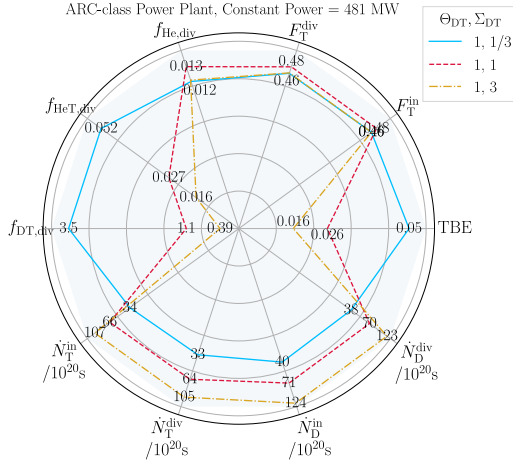
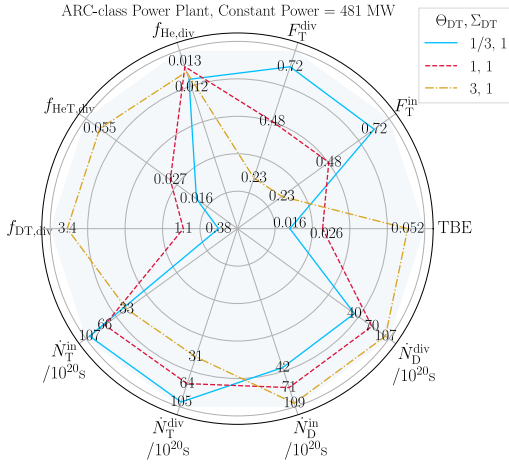
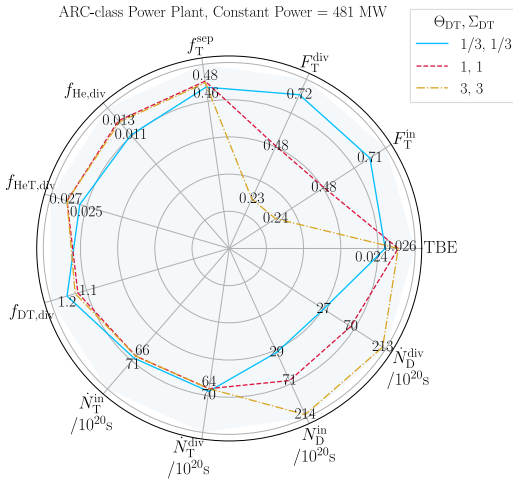
(a) Scan in Σ_{DT} .(b) Scan in Θ_{DT} .(c) Scan in Θ_{DT} and Σ_{DT} .

FIG. 12: Tritium self-sufficiency and fusion power parameters of an ARC-class device for a scan in (a) Σ_{DT} , (b) Θ_{DT} , (c) both Σ_{DT} and Θ_{DT} .

C. Σ_{DT} scan.

In this subsection, we show the effects of changing Σ_{DT} at fixed Θ_{DT} for an ARC-class plant. Shown in Figure 12 (a), decreasing Σ_{DT} from 3 to 1/3 increases the TBE by a factor of 3. Curiously, by noting the change in \dot{N}_T^{in} and \dot{N}_D^{in} , there is roughly a factor of 3 decrease in both D_T and D_D as Σ_{DT} decreases from 3 to 1/3. That is, at fixed power, obtaining the maximum TBE by varying Σ_{DT} , D_D , and D_T approximately satisfy

$$\Sigma_{DT} \sim D_T D_D, \quad D_T \sim D_D \quad (77)$$

The TBE also satisfies $TBE \sim 1/D_T$ as expected from Equation (54). Therefore, by decreasing both deuterium and tritium particle transport at fixed fusion power, the required D-T fueling rates decrease and therefore so does the TBE.

In the next subsection, we show that we obtain the same benefits to TBE by increasing the deuterium transport.

D. Θ_{DT} scan.

In this subsection, we show the effects of changing Θ_{DT} at fixed Σ_{DT} for an ARC-class plant. Shown in Figure 12 (b), increasing Θ_{DT} from 1/3 to 3 increases the TBE by a factor of 3. Therefore, we find the expected scaling

$$\Theta_{DT} \sim D_D/D_T, \quad (78)$$

and the TBE also satisfies

$$TBE \sim 1/D_T, \quad (79)$$

as expected from Equation (54). The scaling in the individual diffusivities approximately satisfies

$$D_D \sim 1/\sqrt{\Theta_{DT}}, \quad D_T \sim \sqrt{\Theta_{DT}}. \quad (80)$$

E. Θ_{DT} and Σ_{DT} scan.

In order to find the dependence of TBE on D_D and D_T , we vary Θ_{DT} and Σ_{DT} simultaneously such that $\Theta_{DT} \sim \Sigma_{DT}$. Shown in Figure 12 (c), the TBE is roughly constant, while D_D varies by a factor of 9. Thus, we find that

$$D_D \sim \Theta_{DT} \Sigma_{DT}. \quad (81)$$

Comparing with Equation (79), the TBE satisfies

$$TBE \sim \Theta_{DT}/\Sigma_{DT}. \quad (82)$$

Therefore, at fixed power we have increased the deuterium particle diffusivity by a factor of 9 but the TBE is still approximately constant because we held the tritium particle diffusivity approximately constant.

We have demonstrated the useful result that the TBE is independent of D_D as long as the divertor pumping scheme can handle the resulting mass flow rates of deuterium and tritium. Thus, increasing deuterium transport while also proportionally increasing pumping deuterium speed does not increase TBE – increased deuterium particle transport must result in a corresponding increase in $f_{DT,div}$ in order for TBE to increase.

This is a useful result for the following reason. Particle transport is constrained by ambipolarity $\sum_s Z_s \Gamma_s = 0$. For a three-species plasma with deuterium, tritium, and electrons,

$$\Gamma_T = \Gamma_e - \Gamma_D. \quad (83)$$

Therefore, if one can decrease $\Gamma_e - \Gamma_D$, for example by increasing Γ_D at fixed Γ_e , one decreases Γ_T . Depending on the density profiles, this may correspond to lower D_T values, and hence higher TBE. More possibilities for manipulating tritium particle transport arise in the presence of impurities, where ambipolarity satisfies

$$\Gamma_T = \Gamma_e - \Gamma_D - \sum_j Z_j \Gamma_j, \quad (84)$$

where the last term is a sum over impurity species.

Therefore, if the fuelling and pumping systems can handle particle flow rates corresponding to changes in deuterium and tritium transport, it may be desirable to increase deuterium particle transport in order to decrease tritium particle transport and therefore increase tritium burn efficiency.

Heuristically, this argument can be demonstrated as follows. Writing Equation (83) as

$$D_T = \frac{\Gamma_e - \Gamma_D}{-\nabla n_T^{co}}, \quad (85)$$

and using $TBE \sim 1/D_T$, we find

$$TBE \sim \frac{-\nabla n_T^{co}}{\Gamma_e - \Gamma_D}. \quad (86)$$

We only consider $-\nabla n_T^{co} > 0$ and $\Gamma_e - \Gamma_D > 0$. Therefore, we arrive at a heuristic prescription for higher TBE: increase D_D and decrease D_T . Actively prevent deuterium from being pumped too quickly from the divertor so that the deuterium density fraction rises, increasing the TBE. As pointed out in [25], deuterium is orders of magnitude cheaper than tritium.

There are many caveats to this statement. In this work, we have assumed that diffusive turbulent transport dominates particle transport. We have assumed that the ratio of D_D/D_T does not have a radial dependence. Higher fidelity models are required to validate the intuition gained from the simple models presented in this work and techniques for intentionally increasing D_D/D_T need to be developed.

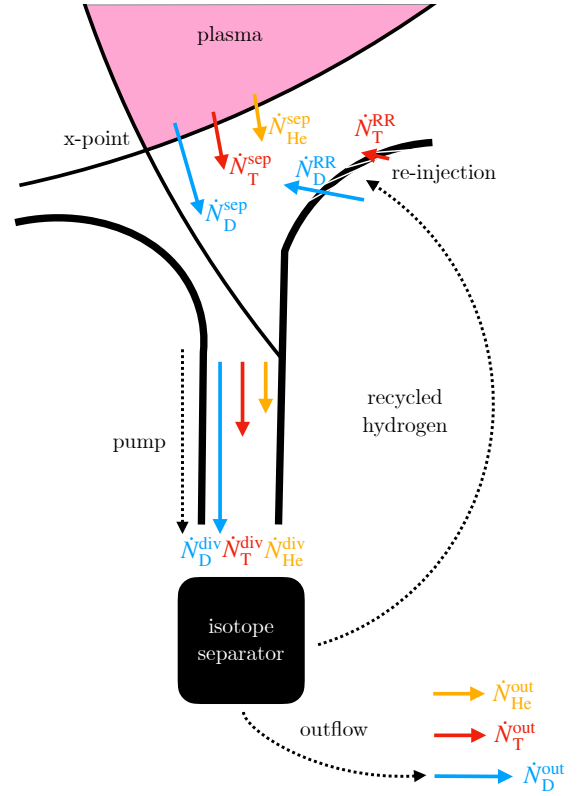


FIG. 13: Schematic of a rapid divertor re-injection scheme.

An isotope separator quickly outputs a deuterium and tritium flow with a tritium fraction $F_T^{RR} = \dot{N}_T^{RR} / \dot{N}_Q^{RR}$, re-injecting particles back into the divertor region.

VII. DEVELOPMENT OF PUMPING TECHNOLOGY

In this section, we describe potential avenues for developing pumping technologies that could facilitate the D-T asymmetric scenarios in this work.

A. Rapid Hydrogen Re-injection

Here, we discuss a rapid hydrogen re-injection (RR) technique for achieving an effect analogous to $\Sigma_{DT} < 1$ without changing the relative D-T pumping speed Σ_{DT} . As in previous sections, the goal is to increase the relative density of deuterium to tritium at the divertor, $f_{DT,div}$. As with improvements in Σ_{DT} discussed earlier, it is important to clarify the causal chain: decreasing Σ_{DT} does not automatically increase TBE, rather, decreases in particle transport can be translated to higher TBE values by deploying technologies that obtain lower Σ_{DT} . We describe this system as ‘rapid’ because the hydrogen is re-injected back into the scrape-off layer much faster than hydrogen leaving through the divertor, being processed in the fuel cycle, and then re-fuelling the plasma.

RR is designed to increase the TBE by increasing the relative helium-tritium divertor density $f_{HeT,div}$. Sup-

Θ_{DT}, Σ_{DT}	P_f (MW)	Q	TBE	$I_{\text{startup,min}}$ (kg)	\tilde{f}_T^{co}	f_T^{sep}	$f_{\text{He,div}}$	\dot{N}_T^{burn} ($10^{20}/\text{s}$)	F_T^{div}	$f_{DT,\text{div}}$	\dot{N}_T^{div} ($10^{20}/\text{s}$)	\dot{N}_D^{div} ($10^{20}/\text{s}$)	F_T^{in}	\dot{N}_T^{in} ($10^{20}/\text{s}$)	$\dot{N}_{D,\text{in}}$ ($10^{20}/\text{s}$)
1/3,3	481	20	0.01	0.80	0.48	0.48	0.01	1.7	0.74	0.12	120	43	0.73	122	45
1,1	481	20	0.03	0.40	0.48	0.48	0.01	1.7	0.48	1.1	64	70	0.48	66	71
5,1/5	481	20	0.29	< 0.01	0.47	0.43	0.01	1.7	0.13	33	4.1	27.1	0.17	5.8	29
1/3,3	38	-	0.60	< 0.01	0.12	0.09	0.69	0.13	0.22	1.2	0.09	0.31	0.33	0.22	0.45
1,1	162	0.51	0.60	< 0.01	0.21	0.15	0.22	0.58	0.15	5.9	0.38	2.3	0.25	0.96	2.84
5,1/5	447	14	0.60	< 0.01	0.44	0.33	0.03	1.6	0.09	51	1.1	10.9	0.18	2.7	12.5
1/3,3	351	5.3	0.10	0.05	0.48	0.51	0.10	1.3	0.76	0.11	11.2	3.6	0.72	12.5	4.87
1,1	415	11	0.10	0.06	0.45	0.45	0.05	1.5	0.45	1.3	13.3	16.5	0.45	14.7	18.0
5,1/5	499	24	0.10	0.07	0.49	0.48	0.00	1.8	0.16	27	16	86.3	0.17	18	88

TABLE I: Key fusion power and tritium self-sufficiency parameters for different operating scenarios in an ARC-class device. In addition to the listed parameters, all cases have $\eta_{\text{He}} = 1.00$, $\Sigma_{\text{HeT}} = 1.00$, $\tau_{\text{FC}} = 4\text{h}$, $\tau_{\text{OFC}} = 24\text{h}$, and $\text{TBR} = 1.08$. Note that $I_{\text{startup,min}}$ values below a certain value are likely not well-described by the model in this work.

pose that once hydrogen is removed from the divertor, the deuterium and tritium can be rapidly separated, and if desired, re-injected back into the divertor at a desired tritium flow rate fraction F_T^{RR} . A technology capable of achieving this – the partial ionization plasma centrifuge – is described in Section VIII B.

A schematic of the RR setup is shown in Figure 13. By re-injecting hydrogen back into the divertor, this modifies the boundary condition $F_T^{\text{div}} = F_T^{\text{sep}}$ (Equation (45)). To determine the new boundary condition, consider the tritium and total hydrogen flows around the separatrix and the divertor

$$\dot{N}_T^{\text{div}} = \dot{N}_T^{\text{sep}} + \dot{N}_T^{\text{RR}}, \quad (87)$$

$$\dot{N}_Q^{\text{div}} = \dot{N}_Q^{\text{sep}} + \dot{N}_Q^{\text{RR}}, \quad (88)$$

where \dot{N}_T^{RR} and \dot{N}_Q^{RR} are the rapidly recycled tritium and total hydrogen flow rates resulting from being re-injected into the divertor. The tritium flow rate of rapidly recycled hydrogen is

$$F_T^{\text{RR}} \equiv \dot{N}_T^{\text{RR}} / \dot{N}_Q^{\text{RR}}, \quad (89)$$

and the fraction of hydrogen entering the divertor that is rapidly recycled is

$$R_Q \equiv \dot{N}_Q^{\text{RR}} / \dot{N}_Q^{\text{div}}. \quad (90)$$

Obtaining $R_Q > 0$ and $F_T^{\text{RR}} \neq F_T^{\text{div}}$ is due to partial ionization plasma centrifuge, described in Section VII B. Combining Equations (87) to (90), the new boundary condition is

$$F_T^{\text{div}} = F_T^{\text{sep}} \kappa, \quad (91)$$

where

$$\kappa \equiv 1 - R_Q \left(1 - \frac{F_T^{\text{RR}}}{F_T^{\text{sep}}} \right). \quad (92)$$

κ is plotted versus R_Q for several $F_T^{\text{RR}}/F_T^{\text{sep}}$ values in Figure 14(a). For $F_T^{\text{RR}}/F_T^{\text{sep}} = 1$, it is intuitive that κ

remains equal to 1 for all R_Q values because the same tritium flow rate fraction is injected back into the divertor. Using Equation (10) for F_T^{co} evaluated at the separatrix,

$$F_T^{\text{sep}} = \frac{f_T^{\text{sep}}}{\Theta_{DT} (\Lambda - f_T^{\text{sep}}) + f_T^{\text{sep}}}, \quad (93)$$

and

$$F_T^{\text{div}} = \frac{1}{1 + f_{DT,\text{div}} \Sigma_{DT}}, \quad (94)$$

we find that the modified tritium-to-deuterium divertor density ratio is

$$f_{DT,\text{div}} = \frac{1}{\Sigma_{DT}} \frac{\Theta_{DT} (\Lambda - f_T^{\text{sep}}) + f_T^{\text{sep}} (1 - \kappa)}{f_T^{\text{sep}} \kappa}. \quad (95)$$

Finally, the hydrogen flow rate out of the system (see Figure 13) is equal to the hydrogen flow across the separatrix

$$\dot{N}_Q^{\text{out}} = \dot{N}_Q^{\text{div}} - \dot{N}_Q^{\text{RR}} = \dot{N}_Q^{\text{sep}}. \quad (96)$$

However, because in general $F_T^{\text{RR}} \neq F_T^{\text{sep}}$, the tritium output flow \dot{N}_T^{out} will be different to \dot{N}_T^{sep} and \dot{N}_T^{div} . In order to recast the effect of rapid hydrogen recycling as an effective D-T pumping ratio, we write Equation (95) as

$$f_{DT,\text{div}} = \frac{1}{\Sigma_{DT}^{\text{RR}}} \frac{1}{\Sigma_{DT}} \frac{\Theta_{DT} (\Lambda - f_T^{\text{sep}})}{f_T^{\text{sep}}}, \quad (97)$$

where

$$\begin{aligned} \Sigma_{DT}^{\text{RR}} &= \kappa \left[1 + \frac{f_T^{\text{sep}} (1 - \kappa)}{\Theta_{DT} (\Lambda - f_T^{\text{sep}})} \right]^{-1} \\ &= \frac{1 + R_Q \left[F_T^{\text{RR}} \Theta_{DT} \left(\frac{\Lambda}{f_T^{\text{sep}}} - 1 \right) + F_T^{\text{RR}} - 1 \right]}{1 - F_T^{\text{RR}} R_Q - \frac{f_T^{\text{sep}} R_Q (F_T^{\text{RR}} - 1)}{\Theta_{DT} (\Lambda - f_T^{\text{sep}})}}. \end{aligned} \quad (98)$$

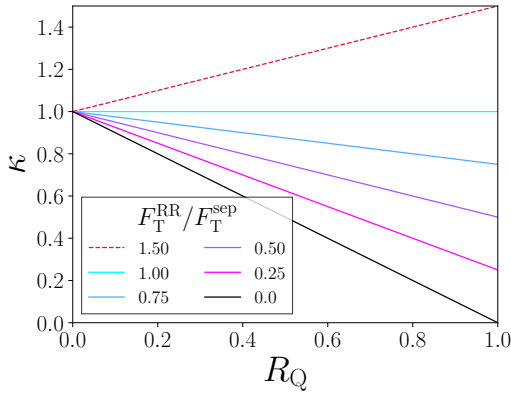
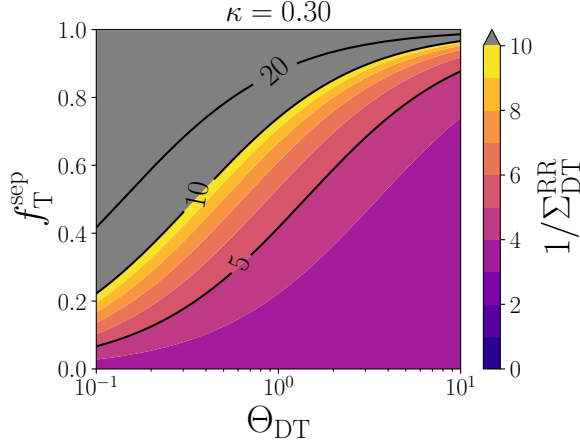
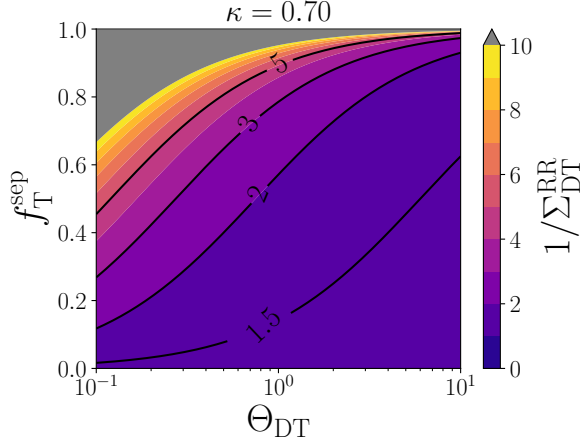
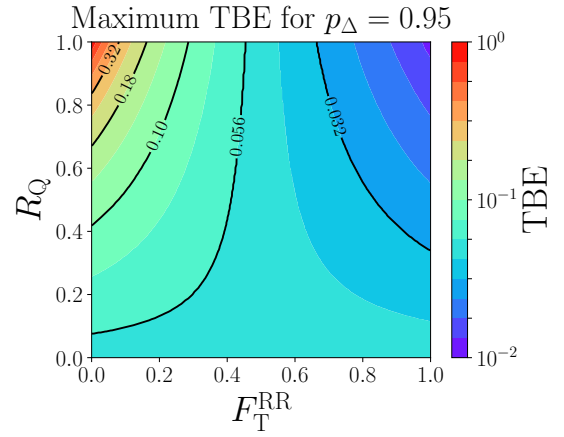
(a) κ .(b) $1/\Sigma_{DT}^{RR}$ for $\kappa = 0.30$.(c) $1/\Sigma_{DT}^{RR}$ for $\kappa = 0.70$.

FIG. 14: Key quantities in a rapid re-injection (RR) system:

(a) κ (Equation (92)) versus R_Q for several F_T^{RR}/F_T^{sep} values, and $1/\Sigma_{DT}^{RR}$ (Equation (98)) versus f_T^{sep} and Θ_{DT} for $\kappa = 0.30$ in (b) and $\kappa = 0.70$ in (c). $\Lambda = \Sigma_{HeT} = \eta_{He} = 1.0$.

In Figure 14(b) and (c), we plot $1/\Sigma_{DT}^{RR}$ versus f_T^{sep} and Θ_{DT} for two κ values. Increasing f_T^{sep} and Θ_{DT} at fixed $\Lambda = 1.0$ always increases Σ_{DT}^{RR} , which means there is a tradeoff between increasing Θ_{DT} and decreasing Σ_{DT}^{RR} .

FIG. 15: Maximum TBE versus F_T^{RR} and R_Q for $p_\Delta = 0.95$, $\Lambda = \Sigma_{HeT} = \eta_{He} = 1.0$.

However, for the parameters considered in Figure 14(b) and (c), the maximum Σ_{DT}^{RR} is κ , which if less than one, can still be very beneficial for TBE and fusion power. Analogous to the earlier discussion on Σ_{DT} and transport, decreasing Σ_{DT}^{RR} also corresponds to a decrease in deuterium and tritium particle transport.

We now study the effects of $R_Q \neq 0$ on ARC-class cases. We assume that $\Sigma_{DT} = 1$, and that all the changes in the TBE and fusion power instead arise from $\Sigma_{DT}^{RR} \neq 1$. The results are shown in Figure 16 for a case with fixed fusion power.

The expression for tritium burn efficiency in Equation (30) is also modified to

$$\text{TBE} = \frac{f_{HeT,div} \Sigma_{HeT}}{\left(1 - \frac{F_T^{RR}}{F_T^{div}} R_Q\right) + f_{HeT,div} \Sigma_{HeT}}. \quad (99)$$

In Figure 15 we plot the maximum TBE (again, optimized over F_T^{in}) versus F_T^{RR} and R_Q . In this case, for $F_T^{RR} < F_T^{div} \simeq 1/2$, increasing R_Q always increases TBE. However, for $F_T^{RR} > F_T^{div} \simeq 1/2$ increasing R_Q always decreases TBE. Very high R_Q values and very small F_T^{RR} values can support a very high TBE of $\text{TBE} \gtrsim 0.3$. Requiring that the denominator of Equation (99) is positive gives the physical constraint that the flow rate of rapidly recycled tritium cannot exceed the tritium injection rate

$$\dot{N}_T^{RR} < \dot{N}_T^{in}, \quad (100)$$

and requiring $\text{TBE} < 1$ gives $\dot{N}_T^{RR} < \dot{N}_T^{div}$.

Shown in Figure 16, we consider four cases with fixed fusion power. The nominal case has zero rapid re-injection and $\text{TBE} = 0.01$. Case A has $R_Q = 0.5$ and $F_T^{RR} = 0.4$ only marginally increases the TBE from 0.026 to 0.028. For case B, $R_Q = 0.5$ and $F_T^{RR} = 0.1$, the TBE increases further to $\text{TBE} = 0.042$ through a combination of $\Sigma_{DT}^{RR} < 1$ and an increase in $f_{HeT,div}$. For case C, $R_Q = 0.8$ and $F_T^{RR} = 0.1$, the TBE increases to

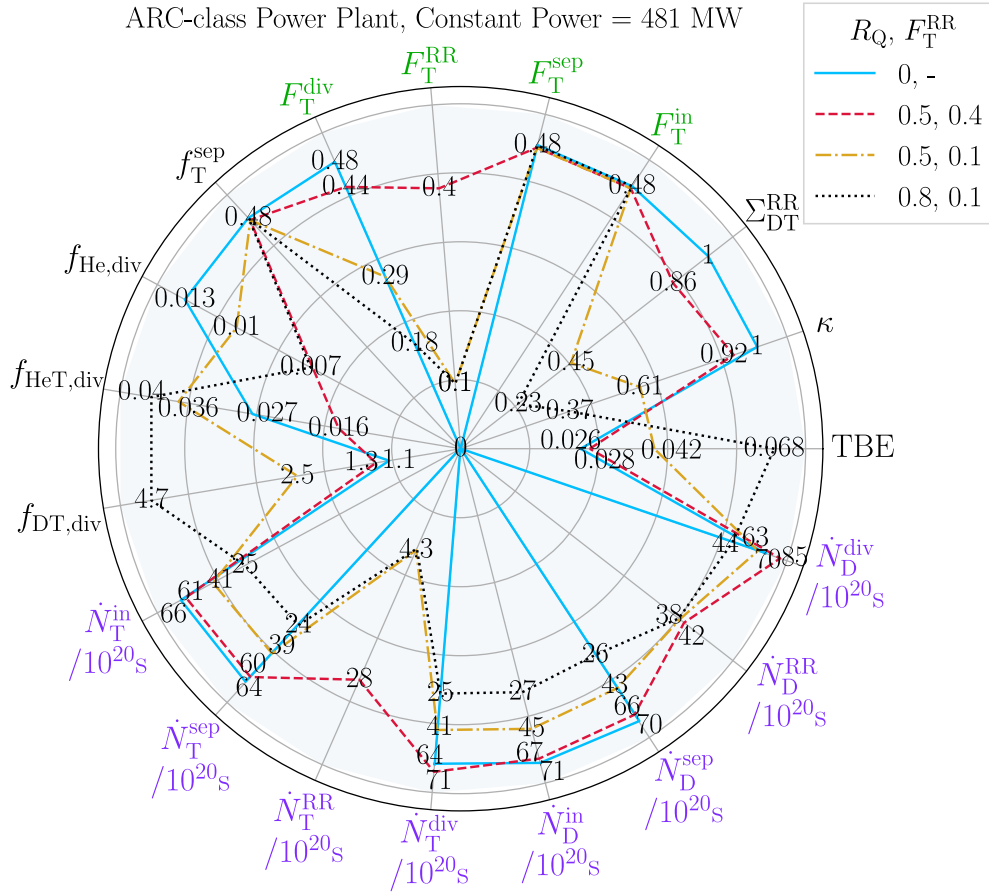


FIG. 16: Tritium self-sufficiency and fusion power parameters of an ARC-class device for four cases with different rapid re-injection parameters and fixed fusion power $P_f = 481$ MW. Axes with titles with font colors different to black are scaled the same as other axis titles of the same color. Some axes are log-scaled, some are linearly scaled.

$$\Theta_{DT} = \Sigma_{DT} = \Sigma_{HeT} = \Lambda = \eta_{He} = 1.0.$$

TBE = 0.068, an almost three-fold improvement over the nominal case.

There are important caveats and future questions to address. As discussed in [4, 11], increasing the helium to hydrogen density assumes that the helium particle confinement time increases. A transport model coupling the plasma core, pedestal, scrape-off-layer, and divertor is needed to more definitively assess the effects of a rapid re-injection scheme.

In summary, we have modeled the effects of a rapid divertor re-injection scheme, shown in Figure 13. By re-injecting deuterium and tritium from the divertor pumped outflow, we demonstrated a factor of three increase in the tritium burn efficiency could be achieved while maintaining constant fusion power. Theoretically, even higher TBE values are possible with extreme R_Q and F_T^{RR} values. Such improvements are mainly obtained by increasing the helium and deuterium density relative to the tritium density at the divertor, while also reducing the tritium fueling fraction.

B. Mass-Selective Pumping with a Partial Ionization Plasma Centrifuge

In this section, we describe a scheme for efficiently separating species by their mass. The separation of hydrogen isotopes is a challenging task due to small differences in the chemical properties between isotopes. Additional constraints are imposed by the requirement to have minimal tritium inventory in the system, which requires short tritium processing times.

The challenge of differential pumping is further increased by the presence of helium, which ideally would be pumped at least at the same rate as tritium, and if possible should be pumped at a higher rate. However, the fact that fully-ionized helium-4 and deuterium nuclei have the same charge-to-mass ratio limits the range of possible separation approaches, especially for concepts operating in a fully ionized plasma. Furthermore, the fact that helium and the deuterium molecule D2 have approximately the same mass means that mass-based separation is infeasible for a fully neutral gas. Therefore, mass-based separation of deuterium and helium is only possible with

R_Q, F_T^{RR}	P_f (MW)	Q	TBE	$I_{\text{startup,min}}$ (kg)	\tilde{f}_T^{co}	f_T^{sep}	$f_{\text{He,div}}$	\dot{N}_T^{burn} ($10^{20}/\text{s}$)	F_T^{div}	$f_{\text{DT,div}}$	\dot{N}_T^{div} ($10^{20}/\text{s}$)	\dot{N}_D^{div} ($10^{20}/\text{s}$)	F_T^{in}	\dot{N}_T^{in} ($10^{20}/\text{s}$)	$\dot{N}_{\text{D,in}}$ ($10^{20}/\text{s}$)
0, -	481	20	0.026	0.40	0.48	0.48	0.01	1.7	0.48	1.1	64	70	0.48	66	71
0.5, 0.4	481	20	0.028	0.37	0.48	0.48	0.01	1.7	0.48	1.3	71	85	0.48	61	67
0.5, 0.1	481	20	0.042	0.23	0.48	0.48	0.01	1.7	0.48	2.5	41	63	0.48	41	45
0.8, 0.1	481	20	0.68	0.12	0.48	0.48	0.01	1.7	0.48	4.7	25	44	0.48	25	27

TABLE II: Key fusion power and tritium self-sufficiency parameters for different operating scenarios in an ARC-class device with rapid re-injection. In all four cases, $\Theta_{\text{DT}} = \Lambda = \Sigma_{\text{HeT}} = \Sigma_{\text{DT}} = 1.0$. More quantities are shown in Figure 16.

atomic, not molecular, deuterium.

The partial ionization plasma centrifuge (PIPC) could enable mass-based separation of hydrogenic species from helium-4 as well as the higher- Z noble gases. It could also enable differential in-situ pumping in the divertor. By primarily operating on atomized neutral hydrogen, a PIPC operates on deuterium and helium atoms, separated by a factor of two in mass and therefore straightforwardly separable.

It can be shown that in an azimuthally symmetric rotating gas, the radial pressure profile $p(r)$ in the gas can be described by [50]

$$p(a)/p(r) = \exp\left(\frac{m}{k_B T} \int_r^a \frac{v_\theta(r')^2}{r'} dr'\right), \quad (101)$$

where p is the partial pressure of the species of mass m in atomic mass units, a is the coordinate of the outermost radius of the device, and $v_\theta(r)$ is the azimuthal velocity of the gas.

We further simplify the problem by assuming that for a rigid body rotation profile, $\omega = v_\theta(r)/r = \text{constant}$. The maximum compression between $r = 0$ and the outer radius at $r = a$ is then

$$p(a)/p(0) = \exp\left(\frac{m v_\theta(a)^2}{2k_B T}\right). \quad (102)$$

Evidently, high compression ratios can be achieved at high rotational velocities and low temperatures, with an especially strong dependence on the rotational velocity.

In a mechanical ultracentrifuge, rotational speeds are ultimately limited by material strength; in contrast, plasma centrifuges operate by driving a radial current through a partially ionized gas inside a background magnetic field, using the ion population as a kind of rotor to spin up the neutrals through collisions. As a result, there are no moving parts and no structural limits to gas velocity. By operating in a partially ionized state, this approach achieves lower temperatures and the relevant physics of the process are simpler than fully ionized plasma centrifuges.

While there are no basic structural limits on operating parameters, there is a velocity limit imposed by the Alfvén ionization limit (or alternatively, the "Critical Ionization Velocity") [51], given by the velocity at which the neutral gas kinetic energy equals the ionization energy of that species.

Furthermore, as noted by prior authors [52] another limit on achievable separation factors in this process is imposed by plasma heating through various mechanisms, including viscous shear, resistive heating, and electron collisions with ions and neutrals.

Still, large differences in compression can be achieved between the relevant isotopes while assuming realistic plasma temperatures, resulting in the capability for differential pumping. As noted in Equation (63), the flow rate of a gas is proportional to both upstream partial pressure of a species and the pumping speed for that species, meaning that species-dependent increases in partial pressure function identically to increases in species-dependent pumping speed. The ratio of tritium to deuterium pumping rates can be written, using Equation (63), as

$$\frac{\dot{N}_T^{\text{out}}}{\dot{N}_D^{\text{out}}} = \frac{1}{\Sigma_{\text{DT}} f_{\text{DT,div}}} R_{\text{sep}}, \quad (103)$$

where R_{sep} is the separation factor [50]

$$R_{\text{sep}} = \exp\left(\frac{(m_T - m_D)v_\theta(a)^2}{2k_B T}\right). \quad (104)$$

In the same way as the rapid re-injection system in Equation (98), R_{sep} can be recast as an effective D-T pumping speed ratio if we assume that all of the deuterium is re-injected into the divertor,

$$\Sigma_{\text{DT}}^{\text{PIPC}} \equiv 1/R_{\text{sep}}. \quad (105)$$

Therefore, Equation (103) becomes

$$\frac{\dot{N}_T^{\text{out}}}{\dot{N}_D^{\text{out}}} = \frac{1}{\Sigma_{\text{DT}}^{\text{PIPC}}} \frac{1}{\Sigma_{\text{DT}} f_{\text{DT,div}}}. \quad (106)$$

Prior work in the field of plasma chemistry has already demonstrated large separation factors in light isotopes, providing some validation that this could be a promising approach to explore. In reference [53], the investigators measured separation factors up to $R_{\text{sep}} \sim 25$ between H_2 and D_2 molecules; because of relative recombination rates this corresponds to a separation factor of 5 between H and D atoms. In the present case where we are concerned with differential pumping of D and T, the same mass difference is present and so the same separation factor could be expected. To compare with a specific case identified

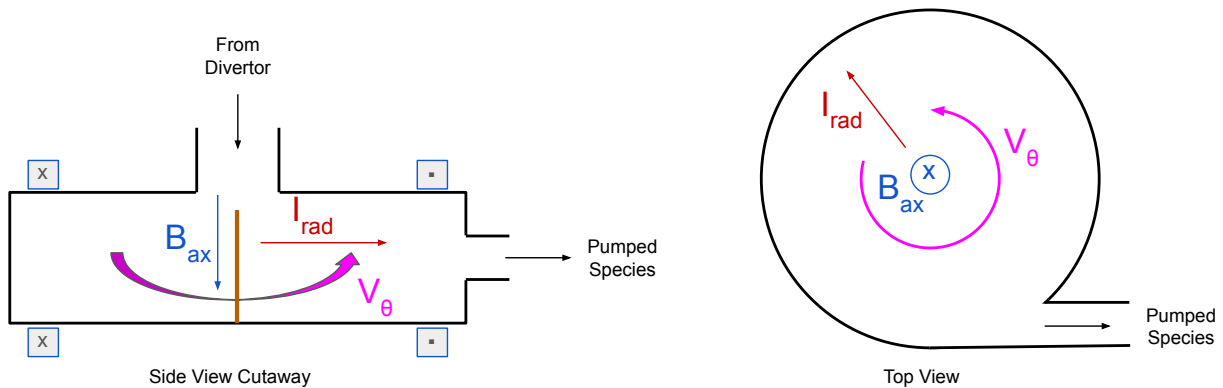


FIG. 17: Schematic view of a plasma centrifuge operating based on azimuthal rotation achieved through a radial current and axial magnetic field.

here, the high-TBE case presented in the third row of Table I requires a separation factor of ~ 6.1 to satisfy the pumping requirement $\Sigma_{DT}^{PIPC} \Sigma_{DT} = 1/5$, demonstrating that the required performance for this application has nearly been achieved in similar experimental conditions.

It should be noted that differentially higher pumping of both tritium and helium relative to deuterium is achieved in this process. The present work has identified the significance of the former, while earlier work [4] emphasized the critical importance of higher helium pumping rates in achieving high TBE at high fusion power density.

Further work could be done to improve these separation factors through improved engineering design to increase azimuthal velocities while limiting the plasma temperature in the device. A future paper will explore some of these methods and discuss early experimental work in progress to develop this device for applications in fusion energy [54].

In addition to the benefits for differential pumping, the value of a tritium compatible divertor pump with no moving parts should not be understated. It is understood that cryosorption pumps have large disadvantages in fusion systems operating for long periods of time including large tritium inventories, inherently pulsed operation, and large recirculating power cost. While diffusion pumps have been explored as primary pumps, mercury usage as the working fluid is prohibited by the Minamata convention [55] and while other authors [56] have proposed using liquid lithium as a working fluid, there have been reports of other alkali metals as the working fluid (K and Na) [57], but not yet demonstrated with Li.

VIII. DISCUSSION

We have introduced two new avenues for operating magnetic confinement fusion power plants with very high tritium burn efficiency, fusion power, and fusion gain: (1)

controlling the physics parameter Θ_{DT} and (2) the engineering parameter Σ_{DT} . Increasing Θ_{DT} causally improves the tritium burn efficiency without compromising fusion power. Decreasing Σ_{DT} is required when both deuterium and tritium particle transport decrease and a high tritium burn efficiency is desired. Without lower values of Σ_{DT} , tritium cannot be exhausted sufficiently quickly for a high tritium burn efficiency to be achieved. This results in a relatively high tritium-to-helium divertor density, corresponding to lower TBE.

Combining high Θ_{DT} and low Σ_{DT} values resulted in an eleven-fold improvement in TBE for an ARC-class power plant with constant fusion power (Figure 1). While this tritium-lean design has a separatrix density comparable to other fusion systems such as MANTA [49], the tritium-lean design's ratio of separatrix deuterium to tritium density is 51:1 – an extremely high value – whereas the ratio is roughly 1:1 in most fusion system designs. At very high fixed TBE = 0.600, the high Θ_{DT} and low Σ_{DT} values resulted in a fusion power of 447 MW versus 162 MW for the nominal case. Introducing a mass-selective pump with a partial ionization plasma centrifuge could enable significant differences in deuterium and tritium pumping speeds.

We have also shown that low Θ_{DT} and high Σ_{DT} values give very poor TBE and fusion power – avoiding operating such regimes is important for commercially viable fusion power systems.

Combined with other proposals for increasing tritium burn efficiency [3, 4, 10, 11, 58], magnetic confinement power plants with very high TBE could be attainable. While we have focused on magnetic confinement fusion, the ideas presented here might lend themselves to other fusion concepts.

It is worth reiterating that while no conclusive evidence exists for very strong asymmetries in particle transport between the main ion species in magnetically confined plasmas, some experimental results hint that strong

Name	Quantity	Units	Equation
Deuterium, tritium, hydrogen flow rate (plasma core)	$\dot{N}_D^{\text{co}}, \dot{N}_T^{\text{co}}, \dot{N}_Q^{\text{co}}$	s^{-1}	eq. (1)
Tritium particle flux density	Γ_T	$\text{m}^{-2}\text{s}^{-1}$	eq. (1)
Deuterium, tritium particle diffusivity	D_D, D_T	m^2s^{-1}	eq. (2)
Deuterium, tritium, hydrogen, electron density (plasma core)	$n_D^{\text{co}}, n_T^{\text{co}}, n_Q^{\text{co}}, n_e^{\text{co}}$	m^{-3}	eq. (2)
Core tritium density fraction	f_T^{co}		eq. (18)
Deuterium-tritium particle diffusivity ratio	$\Theta_{DT} \equiv D_D/D_T$		eq. (7)
Tritium-hydrogen logarithmic density ratio	Λ		eq. (8)
Tritium injection flow rate fraction	$F_T^{\text{in}} \equiv \dot{N}_T^{\text{in}}/\dot{N}_Q^{\text{in}}$		eq. (11)
Tritium divertor removal flow rate fraction	$F_T^{\text{div}} \equiv \dot{N}_T^{\text{div}}/\dot{N}_Q^{\text{div}}$		eq. (12)
Tritium, hydrogen flow rate (divertor)	$\dot{N}_T^{\text{div}}, \dot{N}_Q^{\text{div}}$	s^{-1}	eq. (11)
Tritium flow rate enrichment	H_T		eq. (13)
Fusion power	P_f	W	
D-T fusion energy release	E	J	eq. (34)
Fusion power density	p_f	W m^{-3}	eq. (34)
D-T fusion reactivity	$\langle v\sigma \rangle$	m^3s^{-1}	eq. (34)
Tritium burn rate	\dot{N}_T^{burn}	s^{-1}	eq. (14)
Tritium burn fraction	f_{burn}		eq. (14)
Helium ash removal rate	$\dot{N}_{\text{He}}^{\text{div}}$	s^{-1}	eq. (17)
Tritium burn efficiency	$\text{TBE} \equiv \dot{N}_T^{\text{burn}}/\dot{N}_T^{\text{in}}$		eq. (17)
Divertor neutral pumping speed for species x	S_x	m^3s^{-1}	eq. (27)
Helium-to-fuel divertor density ratio	$f_{\text{He,div}}$		eq. (38)
Helium-to-electron core density ratio	f_{dil}		eq. (32)
Power density multiplier	p_{Δ}		eq. (36)
Helium density enrichment	η_{He}		eq. (37)
D-T pumping speed ratio	$\Sigma_{DT} \equiv S_D/S_T$		eq. (47)
D-T divertor density ratio	$f_{DT,\text{div}}$		eq. (40)
He-T pumping speed ratio	$\Sigma_{\text{HeT}} \equiv S_{\text{He}}/S_T$		eq. (28)
He-T divertor density ratio	$f_{\text{HeT,div}}$		eq. (29)
Plasma gain	Q		eq. (56)
Energy confinement time	τ_E	s	eq. (56)
Constant plasma gain multiplication factor	C		eq. (62)
Separatrix to divertor tritium fraction flow rate ratio	κ		eq. (92)
Tritium rapid re-injection flow rate fraction	$F_T^{\text{RR}} \equiv \dot{N}_T^{\text{RR}}/\dot{N}_Q^{\text{RR}}$		eq. (92)
Hydrogen rapid re-injection to divertor flow rate fraction	$R_Q \equiv \dot{N}_Q^{\text{RR}}/\dot{N}_Q^{\text{div}}$		eq. (92)
Centrifuge separation factor	R_{sep}		eq. (104)

TABLE III: Key quantities used in this work.

asymmetries may exist. [15] reported a mass-dependent particle diffusivity for hydrogen and deuterium in JET experiments, using a diffusive transport model. Furthermore, [16] identified even greater differences in hydrogen and deuterium diffusivities at JET, both at the plasma edge and extending toward the core, with hydrogen diffusivity D_H being up to ten times larger than D_D . This finding is encouraging for D-T operations, as it suggests that achieving $\Theta_{DT} \gg 1$ may be possible with current experimental techniques. Additionally, [17] found that gyrokinetic transport models could not accurately predict the edge tritium density profiles in JET plasmas, potentially hinting at a mass-dependent particle diffusivity for deuterium and tritium. Analysis of relative D-T transport in the first D-T experiments on JET was inconclusive, though it did not exclude the possibility of a mass dependence in the diffusivities of deuterium and tritium. Although [13] did not explicitly analyze deuterium and tritium particle diffusivities, it did reveal a strong dependence of electron particle diffusivity D_e on

the D-T fuel mixture. Upcoming D-T burning plasma experiments, such as SPARC and ITER [1, 2], as well as ongoing magnetic confinement experiments with multiple main ion species, offer potential opportunities to explore and drive asymmetric D-T transport. The values of $\Theta_{DT} \gg 1$ shown to be desirable in this paper would require an extremely strong (and unrealistic with current techniques) dependence on the relative D-T masses, likely requiring new techniques to achieve.

IX. ACKNOWLEDGEMENTS

We are grateful to M. Parsons and J. A. Schwartz for helpful discussions. The US Government retains a non-exclusive, paid-up, irrevocable, world-wide license to publish or reproduce the published form of this manuscript, or allow others to do so, for US Government purposes.

X. DATA AVAILABILITY STATEMENT

The data that support the findings of this study will be made openly available.

Appendix A: Effect of Λ

In this appendix, show the effect of different Λ (Equation (8)) values on the total fusion power. Recall that

$\Lambda \equiv L_{n,T}/L_{n,Q}$. Therefore, we generally expect that plasmas with lower tritium fraction satisfy $\Lambda \gtrsim 1$ because the total hydrogen densities need to be larger than just for tritium. The maximum p_Δ value is found over F_T^{in} . Shown in Figure 18, the maximum p_Δ value is plotted versus Θ_{DT} and Σ_{DT} . Higher values of Λ always lead to higher p_Δ values.

-
- [1] R. Aymar, P. Barabaschi, and Y. Shimomura, *Plasma Physics and Controlled Fusion* **44**, 519 (2002).
- [2] A. J. Creely, M. J. Greenwald, S. B. Ballinger, D. Brunner, J. Canik, J. Doody, T. Fülöp, D. T. Garnier, R. Granetz, T. K. Gray, C. Holland, N. T. Howard, J. W. Hughes, J. H. Irby, V. A. Izzo, G. J. Kramer, A. Q. Kuang, B. LaBombard, Y. Lin, B. Lipschultz, N. C. Logan, J. D. Lore, E. S. Marmor, K. Montes, R. T. Mumgaard, C. Paz-Soldan, C. Rea, M. L. Reinke, P. Rodriguez-Fernandez, K. Särkimäki, F. Sciortino, S. D. Scott, A. Snicker, P. B. Snyder, B. N. Sorbom, R. Sweeney, R. A. Tinguely, E. A. Tolman, M. Umansky, O. Vallhagen, J. Varje, D. G. Whyte, J. C. Wright, S. J. Wukitch, and J. Zhu, *Journal of Plasma Physics* **86** (2020).
- [3] M. Abdou, M. Riva, A. Ying, C. Day, A. Loarte, L. R. Baylor, P. Humrickhouse, T. F. Fuerst, and S. Cho, *Nuclear Fusion* **61**, 10.1088/1741-4326/abbf35 (2021).
- [4] D. Whyte, R. Delaporte-Mathurin, S. Ferry, and S. Meschini, *Nuclear Fusion* **63**, 10.1088/1741-4326/acf3fb (2023).
- [5] S. Meschini, S. E. Ferry, R. Delaporte-Mathurin, and D. G. Whyte, *Nuclear Fusion* **63**, 10.1088/1741-4326/acf3fc (2023).
- [6] J.-P. Girard, P. Garin, N. Taylor, J. Uzan-Elbez, L. Rodríguez-Rodrigo, and W. Gulden, *Fusion Engineering and Design* **82**, 506 (2007), proceedings of the 24th Symposium on Fusion Technology.
- [7] P. W. Humrickhouse and B. J. Merrill, *Fusion Engineering and Design* **135**, 302 (2018), special Issue: FESS-FNSF Study.
- [8] M. J. B. W. S. R. I. C. S. S. H. B. D. R. T. W. K. A. S. W. D. B. Stephen Strikwerda, Paul A. Staniec and R. Lawless, *Fusion Science and Technology* **80**, 607 (2024), <https://doi.org/10.1080/15361055.2023.2210277>.
- [9] T. Tanabe, *Journal of Nuclear Materials* **438**, S19 (2013), proceedings of the 20th International Conference on Plasma-Surface Interactions in Controlled Fusion Devices.
- [10] A. H. Boozer, *Nuclear Fusion* **61**, 10.1088/1741-4326/ac170f (2021).
- [11] J. Parisi, A. Diallo, and J. Schwartz, *Nuclear Fusion* **64**, 126019 (2024).
- [12] B. Balet, P. M. Stubberfield, D. Borba, J. G. Cordey, N. Deliyanakis, C. M. Greenfield, T. T. Jones, R. König, F. B. Marcus, M. F. Nave, D. P. O'Brien, F. Porcelli, G. J. Sadler, K. Thomsen, and M. V. Hellermann, *Nuclear Fusion* **33**, 10.1088/0029-5515/33/9/I09 (1993).
- [13] S. D. Scott, M. C. Zarnstorff, C. W. Barnes, R. Bell, N. L. Bretz, C. Bush, Z. Chang, D. Ernst, R. J. Fonck, L. Johnson, *et al.*, *Physics of Plasmas* **2**, 2299 (1995).
- [14] M. Keilhacker, A. Gibson, C. Gormezano, P. Lomas, P. Thomas, M. Watkins, P. Andrew, B. Balet, D. Borba, C. Challis, I. Coffey, G. Cottrell, H. D. Esch, N. Deliyanakis, A. Fasoli, C. Gowers, H. Guo, G. Huysmans, T. Jones, W. Kerner, R. König, M. Loughlin, A. Maas, F. Marcus, M. Nave, F. Rimini, G. Sadler, S. Sharapov, G. Sips, P. Smeulders, F. Söldner, A. Taroni, B. Tubbing, M. von Hellermann, D. Ward, and J. Team, *Nuclear Fusion* **39**, 209 (1999).
- [15] C. F. Maggi, H. Weisen, J. C. Hillesheim, A. Chankin, E. Delabie, L. Horvath, F. Auriemma, I. S. Carvalho, G. Corrigan, J. Flanagan, L. Garzotti, D. Keeling, D. King, E. Lerche, R. Lorenzini, M. Maslov, S. Menmuir, S. Saarelma, A. C. C. Sips, E. R. Solano, E. Belonohy, F. J. Casson, C. Challis, C. Giroud, V. Parail, C. Silva, M. Valisa, and J. Contributors, *Plasma Physics and Controlled Fusion* **60** (2018).
- [16] L. Horvath, C. Maggi, A. Chankin, S. Saarelma, A. Field, S. Aleiferis, E. Belonohy, A. Boboc, G. Corrigan, E. Delabie, J. Flanagan, L. Frassinetti, C. Giroud, D. Harting, D. Keeling, D. King, M. Maslov, G. Matthews, S. Menmuir, S. Silburn, J. Simpson, A. Sips, H. Weisen, K. Gibson, and J. Contributors, *Nuclear Fusion* **61**, 046015 (2021).
- [17] T. Tala, A. E. Järvinen, C. F. Maggi, P. Mantica, A. Mariani, A. Salmi, I. S. Carvalho, A. Chomiczewska, E. Delabie, F. Devasagayam, J. Ferreira, W. Gromelski, N. Hawkes, L. Horvath, J. Karhunen, D. King, A. Kirjasuo, E. Kowalska-Strzeciwiłk, S. Leerink, M. Lennholm, B. Lomanowski, M. Maslov, S. Menmuir, R. B. Morales, R. Sharma, H. Sun, and K. Tanaka, *Nuclear Fusion* **63**, 10.1088/1741-4326/acea94 (2023).
- [18] C. Estrada-Mila, J. Candy, and R. E. Waltz, *Physics of Plasmas* **12**, 10.1063/1.1848544 (2005).
- [19] E. A. Belli, J. Candy, and R. E. Waltz, *Phys. Rev. Lett.* **125**, 015001 (2020).
- [20] E. A. Belli and J. Candy, *Physics of Plasmas* **28**, 10.1063/5.0048620 (2021).
- [21] J. Garcia, F. J. Casson, A. B. Navarro, N. Bonanomi, J. Citrin, D. King, P. Mantica, A. Mariani, M. Marin, S. Mazzi, E. Viezzer, and J. Contributors, *Plasma Physics and Controlled Fusion* **64**, 054001 (2022).
- [22] N. J. Fisch, *Physics of Plasmas* **2**, 10.1063/1.871454 (1995).

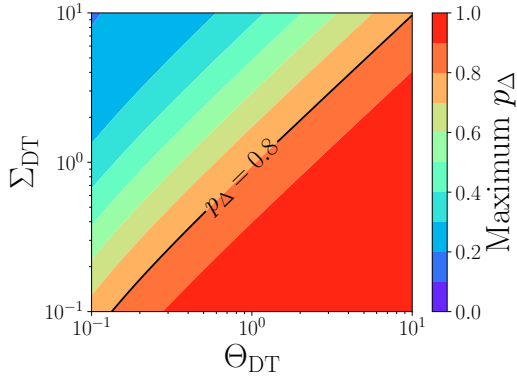
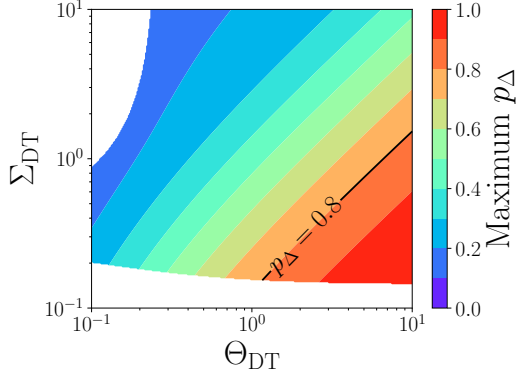
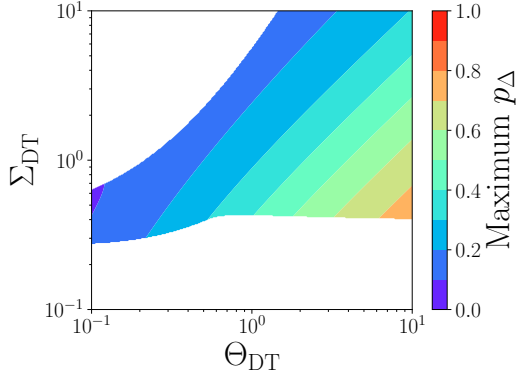
(a) $\Lambda = 4.0$.(b) $\Lambda = 1.0$.(c) $\Lambda = 0.5$.

FIG. 18: Effect of Λ (Equation (8)), Θ_{DT} , and Σ_{DT} on fusion power multiplier p_{Δ} at TBE = 0.40. Here, p_{Δ} is maximized over all F_T^{in} values.

[23] R. White, F. Romanelli, F. Cianfrani, and E. Valeo, *Physics of Plasmas* **28**, 10.1063/5.0033497 (2021).
 [24] M. Tokar and S. Moradi, *Nuclear Fusion* **51**, 063013 (2011).
 [25] A. H. Boozer, *Stellarators with enhanced tritium confinement and edge radiation control* (2024), arXiv:2402.08694 [physics.plasm-ph].
 [26] P. C. Souers, *Hydrogen properties for fusion energy* (Univ of California Press, 1986).
 [27] H. S. Nalwa, *Handbook of surfaces and interfaces of materials, five-volume set* (Elsevier, 2001).

[28] H. Iwahara, *Solid State Ionics* **125**, 271 (1999).
 [29] T. Teichmann and C. Day, *Fusion Engineering and Design* **169**, 112694 (2021).
 [30] J. Weiland, A. Jarmén, and H. Nordman, *Nuclear Fusion* **29**, 1810 (1989).
 [31] S. Mordijck, *Nuclear Fusion* **60**, 10.1088/1741-4326/ab8d04 (2020).
 [32] P. J. Catto, *Plasma Physics* **20**, 719 (1978).
 [33] E. A. Frieman and L. Chen, *The Physics of Fluids* **25**, 502 (1982).
 [34] F. I. Parra and P. J. Catto, *Plasma Physics and Controlled Fusion* **50**, 065014 (2008).
 [35] I. G. Abel, G. G. Plunk, E. Wang, M. Barnes, S. C. Cowley, W. Dorland, and A. A. Schekochihin, *Reports on Progress in Physics* **76**, 116201 (2013).
 [36] C. Day and T. Giegerich, *Fusion Engineering and Design* **88**, 616 (2013), proceedings of the 27th Symposium On Fusion Technology (SOFT-27); Liège, Belgium, September 24-28, 2012.
 [37] S. K. Combs and L. R. Baylor, *Fusion Science and Technology* **73**, 493 (2018).
 [38] L. R. Baylor, S. K. Combs, T. C. Jernigan, W. A. Houlberg, L. Owen, D. Rasmussen, S. Maruyama, and P. Parks, *Physics of plasmas* **12** (2005).
 [39] L. R. Baylor, S. K. Combs, R. C. Duckworth, M. S. Lytle, S. J. Meitner, D. A. Rasmussen, and S. Maruyama, *IEEE Transactions on Plasma Science* **44**, 1489 (2016).
 [40] C. Day, D. Brennan, P. Camp, H. Jensen, G. Jones, A. Mack, and A. Miller, *Fusion science and technology* **48**, 29 (2005).
 [41] A. Mack, A. Antipenkov, J. Boissin, C. Day, S. Gross, H. Haas, V. Hauer, D. Murdoch, and T. Waldenmaier, *Fusion engineering and design* **61**, 611 (2002).
 [42] M. Abdou, M. Riva, A. Ying, C. Day, A. Loarte, L. Baylor, P. Humrickhouse, T. F. Fuerst, and S. Cho, *Nuclear fusion* **61**, 013001 (2020).
 [43] C. Day, (2007).
 [44] W. G. Graham and L. Ruby, *Journal of Vacuum Science and Technology* **16**, 927 (1979).
 [45] C. Day, K. Battes, B. Butler, S. Davies, L. Farina, A. Frattolillo, R. George, T. Giegerich, S. Hanke, T. Härtl, *et al.*, *Fusion Engineering and Design* **179**, 113139 (2022).
 [46] C. Day and T. Giegerich, *Fusion Engineering and Design* **88**, 616 (2013).
 [47] S. Yamaguchi, K. Mukai, J. Yagi, and S. Konishi, *IEEE Transactions on Plasma Science* **50**, 4262 (2022).
 [48] S. Meschini, S. E. Ferry, R. Delaporte-Mathurin, and D. G. Whyte, *Nuclear Fusion* **63**, 126005 (2023).
 [49] T. M. Collaboration, G. Rutherford, H. S. Wilson, A. Saltzman, D. Arnold, J. L. Ball, S. Benjamin, R. Biela-jew, N. de Boucaud, M. Calvo-Carrera, R. Chandra, H. Choudhury, C. Cummings, L. Corsaro, N. DaSilva, R. Diab, A. R. Devitre, S. Ferry, S. J. Frank, C. J. Hansen, J. Jerkins, J. D. Johnson, P. Lunia, J. van de Lindt, S. Mackie, A. D. Maris, N. R. Mandell, M. A. Miller, T. Mouratidis, A. O. Nelson, M. Pharr, E. E. Peterson, P. Rodriguez-Fernandez, S. Segantin, M. Tobin, A. Velberg, A. M. Wang, M. Wigram, J. Witham, C. Paz-Soldan, and D. G. Whyte, *Plasma Physics and Controlled Fusion* **66**, 105006 (2024).
 [50] M. Grossman and T. Shepp, *IEEE Transactions on Plasma Science* **19**, 1114 (1991).
 [51] H. Alfvén, *Rev. Mod. Phys.* **32**, 710 (1960).

- [52] M. M. B. Wijnakker and E. H. A. Granneman, *Zeitschrift für Naturforschung A* **35**, 883 (1980).
- [53] S. V. Korobtsev, T. A. Kosinova, Y. R. Rakhimbabaev, and V. D. Rusanov, *Plasma Chemistry and Plasma Processing* **6**, 97 (1986).
- [54] A. Rutkowski, In preparation.
- [55] Decision adopted by the fourth meeting of the Conference of the Parties to the Minamata Convention on Mercury MC-4/3: Review and amendment of annexes A and B to the Minamata Convention on Mercury (2022).
- [56] C. Baus, P. Barron, A. D'Angiò, Y. Hirata, S. Konishi, J. Mund, T. Nagao, D. Nakahara, R. Pearson, M. Sakaguchi, K. Sakamoto, K. Seko, S. Takeda, A. Wilson, and Y. Yoshioka, *Journal of Fusion Energy* **42**, 10 (2023).
- [57] J. Yagi, Y. Matsunaga, M. Tabuchi, Y. Sugita, Y. Kajimura, K. Mukai, C. Baus, Y. Kume, and S. Konishi, *Fusion Engineering and Design* **202**, 114352 (2024).
- [58] H. Xie, V. S. Chan, R. Ding, N. Shi, X. Jian, R. Zagórski, I. Ivanova-Stanik, J. Chen, J. Chen, J. Li, and the CFETR team, *Nuclear Fusion* **60**, 046022 (2020).